Review | Open Access

Microstructures

Chun *et al. Microstructures* **2026**, *6*, 2026087 **DOI:**10.20517/microstructures.2025.183

Oxide nanostructures for artificial olfaction

Suk Yeop Chun[1,2], Hyun Yeop Cho[3], Hyung Jin Shin[3], Chong-Yun Kang[1,2], Jung Ho Yoon[3]

Keywords:
Gas sensor, oxide, chemoresistive, chemo-memristive, nanostructure, neuromorphic, olfactory system

Citation: Chun, S. Y.; Cho, H. Y.; Shin, H. J.; Kang, C. Y.; Yoon, J. H. Oxide nanostructures for artificial olfaction. *Microstructures* **2026**, *6*, 2026087. https://dx.doi.org/10.20517/microstructures.2025.183

Received: 31 Dec 2025 **First Decision:** 29 Jan 2026 **Revised:** 4 Feb 2026 **Accepted:** 13 Feb 2026 **Published:** 26 Jun 2026

Academic Editor: Zaiping Guo
Copy Editor: Shu-Yuan Duan
Production Editor: Shu-Yuan Duan

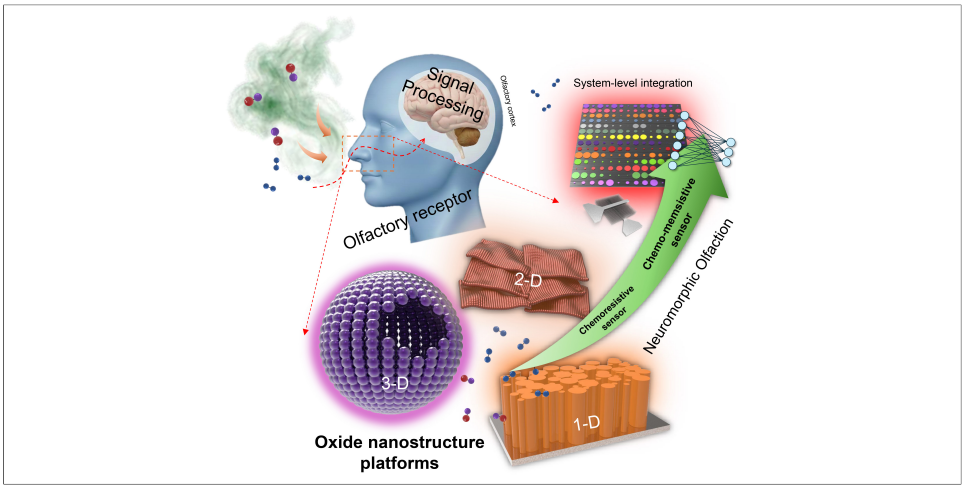

Abstract

Artificial olfaction, inspired by biological sensory systems, offers new opportunities in environmental, industrial, and healthcare applications. Semiconducting metal oxide based chemoresistive gas sensors provide a scalable and core interface for chemical detection and therefore constitute the most extensively explored front end for artificial olfactory systems. Nevertheless, conventional chemoresistive sensing that relies on surface charge transfer remains constrained by incomplete response and recovery, humidity interference, cross selectivity, and strong temperature dependence. This review surveys material- and device-level strategies developed to address these bottlenecks, with an emphasis on nanostructuring approaches that improve gas accessibility and reaction kinetics. Moving beyond device-level performance, the review further situates oxide-based gas sensing within a hierarchical neuromorphic olfactory framework. In biological systems, chemical information is represented by distributed activation patterns and temporal dynamics that extend beyond individual receptor responses. Within this broader context, emerging oxide-based transduction concepts that extend conventional chemoresistive operation are also discussed. Recent artificial olfactory system studies have begun to explore alternative oxide-based transduction mechanisms that extend beyond conventional chemoresistive operation. Among these emerging approaches, chemo-memristive responses based on

[1]KU-KIST Graduate School of Converging Science and Technology, Korea University, Seoul 02841, Republic of Korea.
[2]Electronic and Hybrid Materials Research Center, Korea Institute of Science and Technology (KIST), Seoul 02791, Republic of Korea.
[3]School of Advanced Materials Science and Engineering, Sungkyunkwan University, Suwon 16419, Republic of Korea.

Correspondence to: Dr. Chong-Yun Kang, Electronic and Hybrid Materials Research Center, Korea Institute of Science and Technology (KIST), Seoul 02791, Republic of Korea. E-mail: cykang@kist.re.kr; Prof. Jung Ho Yoon, School of Advanced Materials Science and Engineering, Sungkyunkwan University, Suwon 16419, Republic of Korea. E-mail: junghoyoon@skku.edu

vacancy-mediated ion redox processes are briefly discussed as one possible pathway toward more tightly coupled sensing and signal encoding at the device level. Such developments reflect ongoing efforts to more closely couple sensing and signal processing at the device level. By integrating insights from nanostructured oxide sensors and neuromorphic encoding principles, this review outlines conceptual pathways toward artificial olfactory systems that extend beyond standalone gas detection toward more integrated sensory information processing architectures.

INTRODUCTION

Biological olfaction offers a natural model of chemical recognition, where sensing and processing are closely intertwined. Odorant molecules are detected by receptor neurons in the epithelium; their signals converge onto glomeruli in the olfactory bulb, and synaptic interactions implement combinatorial coding and adaptive plasticity[1,2]. In this way, detection, patterning, and learning occur within the same network, illustrating how complex recognition can emerge from the coordinated action of neurons and synapses. Artificial olfaction aims to realize comparable functionality in engineered systems. In such systems, gas sensors constitute the primary interface to chemical stimuli and define the front-end constraints on sensitivity, selectivity, temporal response, stability, and energy consumption. A range of sensing modalities has been explored, including electrochemical[3], optical[4], acoustic[5], and catalytic combustion[6] approaches. Among these, chemoresistive sensing based on semiconducting metal oxides (SMO) has become a dominant platform owing to its compatibility with complementary metal-oxide-semiconductor (CMOS) fabrication, scalability to dense sensor arrays, and suitability for continuous operation with relatively simple monolithic integration[7-10].

Extensive efforts have therefore been devoted to improving the performance of SMO-based chemoresistive sensors through material and structural engineering. In particular, oxide channels have been engineered into nanostructured forms to enhance surface accessibility and facilitate gas-solid interactions[11,12]. Catalytic decoration using noble metal additives has been widely employed to accelerate surface reactions, enhance sensitivity, and modulate selectivity[13,14]. Together, these approaches have substantially advanced receptor-level transduction performance and established nanostructured and catalyst-modified SMO as the state of the art in gas sensing.

Despite these advances, SMO-based chemoresistive sensors intrinsically exhibit several limitations, including slow and often incomplete response and recovery, cross-selectivity among analytes, strong dependence on operating temperature, and sensitivity to environmental factors such as humidity[15-17]. While nanostructuring and catalytic decoration have significantly mitigated these issues, they cannot be entirely eliminated within the conventional chemoresistive sensing framework. These limitations reflect fundamental characteristics of SMO materials and their operating principles.

The functional demands of artificial olfaction extend beyond improved receptor-level transduction. Discriminating complex odor mixtures, organizing sensor responses into structured representations, and incorporating stimulus history require higher-level interpretation of sensory signals. In many current implementations, including sensor-neuron hybrid systems, these functions are implemented at the system level through explicit circuit or architectural design, while the sensing element itself primarily serves as a transducer. In parallel with ongoing system-level neuromorphic efforts, a range of oxide-based transduction concepts has been explored within artificial olfactory systems to modestly extend the functional role of sensing elements beyond conventional chemoresistive operation. These studies include observations of history-dependent electrical responses associated with vacancy-mediated ion redox processes rather than purely surface charge transfer[18,19]. Considered alongside architectural and circuit-level approaches, such device-level behaviors represent one of several complementary directions being investigated to more closely integrate chemical sensing and signal representation in artificial olfaction.

Biological olfaction provides a reference framework in which sensing and processing are inherently intertwined. Neuromorphic approaches have therefore attracted growing interest as a means to complement advances in SMO gas sensors by providing a hierarchical framework that links receptor-level transduction with higher-level representation and interpretation of chemical information across the system architecture. Such approaches expand the functional scope of artificial olfaction beyond standalone detection without negating material- and device-level advances in gas sensing.

This review first surveys advances in nanostructured and catalyst-modified SMO-based chemoresistive sensors, focusing on how material and surface engineering have improved receptor-level sensing performance and on the intrinsic limitations that remain within conventional transduction frameworks. The discussion then broadens to neuromorphic artificial olfaction, situating oxide-based gas sensing within architectures that address the representation and interpretation of chemical information at the system level. Through this organization, the review clarifies how progress in SMO gas sensing can be positioned within a broader framework for artificial olfactory function.

OXIDE NANOSTRUCTURE GAS SENSORS: PRINCIPLES AND CURRENT ADVANCES

Biological Olfactory Processing and Key Features for Practical Artificial Olfaction

Neuromorphic artificial olfaction requires more than simply detecting odorant molecules; it depends on reproducing the biological strategies by which chemical stimuli are transformed into electrical signals and subsequently processed through neuronal and synaptic interactions[20,21]. Figure 1 situates artificial olfaction within the broader context of biological sensory information processing, showing where current gas sensing research aligns with this hierarchy and where it diverges.

At the early sensory stage, olfactory processing is initiated in the nasal epithelium and olfactory bulb, as shown in Figure 1A. Olfactory receptor neurons (ORNs) express receptor proteins on their ciliary membranes, where odorant binding triggers electrical activity. Action potentials generated in ORNs propagate along their axons and converge in the olfactory bulb. Axons from ORNs carrying the same receptor type terminate in a common glomerulus, thereby organizing distributed sensory inputs into spatially localized centers[22]. This convergence provides a representative example of how chemically diverse stimuli are structured at the receptor level in biological sensory systems.

Within this biological framework, most artificial olfaction platforms have been developed with a strong emphasis on this initial transduction stage. As illustrated in Figure 1B, gas sensors primarily function as artificial receptors that convert chemical stimuli into electrical signals, typically measured as resistance or current changes. Accordingly, receptor-level transduction represents the stage that has been most extensively studied in gas sensing research, with extensive efforts devoted to improving sensitivity, selectivity, response and recovery characteristics, long-term stability, and power efficiency[23,24]. In most current systems, processing beyond this stage is realized through peripheral circuitry or software, rather than through hardware-level integration close to the sensing front end.

The overall organization of biological sensory information processing is summarized in Figure 1C, which depicts a general sensory pathway from peripheral stimulus reception through neuronal connections and synaptic interfaces toward higher brain regions[25]. Although illustrated using the olfactory system, this schematic reflects principles common across sensory modalities, linking receptor-level transduction with downstream neural signaling and synaptic modulation within a unified processing flow.

Beyond simple transduction, biological sensory systems rely on distributed encoding. As shown in Figure 1D, odor identity is encoded through the simultaneous activation of multiple receptor types, generating high-dimensional activity patterns. Such combinatorial coding enables the discrimination of structurally

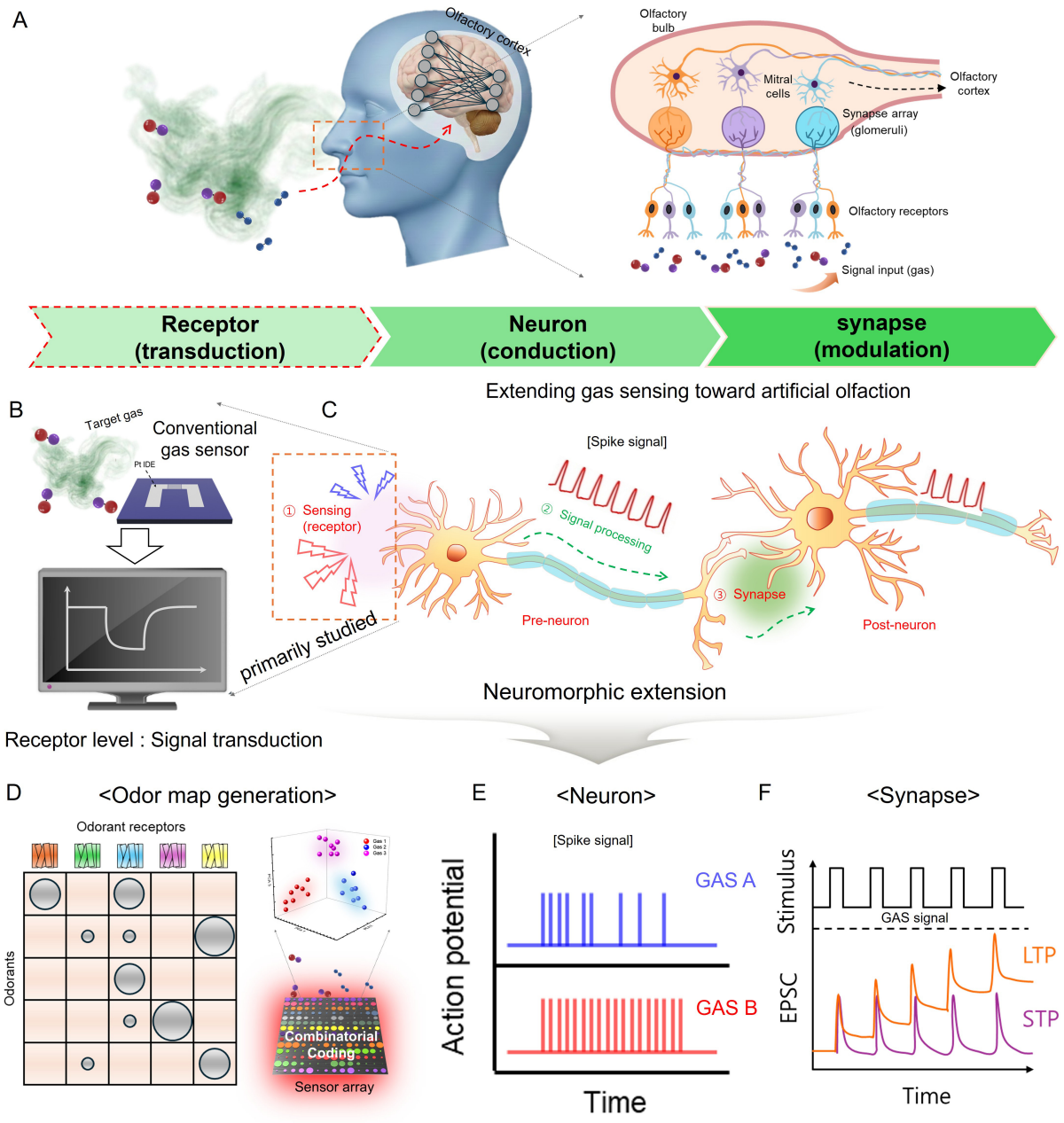

Figure 1. (A) Diagram of the biological olfactory system showing odorant receptors, signal transduction to glomeruli, and processing in the olfactory bulb; (B) Conventional gas sensor architecture emphasizing receptor-level signal transduction, where gas-induced resistance changes are mainly analyzed through steady-state electrical responses; (C) Neuromorphic extension of gas sensing through the integration of receptor-level sensing with neuron- and synapse-inspired spike processing; (D) Unique pattern generation through combinatorial coding, where different odorants activate distinct sets of receptors and generate characteristic response patterns; (E) Illustration of neuron-inspired signal encoding, in which different gas stimuli are represented by stimulus-dependent spike trains over time; (F) Illustration of synaptic weight modulation with stimulus frequency driving short term potentiation(STP) or long term potentiation(LTP). EPSC: Excitatory postsynaptic current.

similar odorants and the recognition of complex mixtures, even when individual receptors exhibit broad and overlapping selectivity[26]. In artificial systems, this principle is mirrored by sensor arrays composed of elements with distinct response characteristics, where the collective response pattern, rather than any single sensor output, forms the basis for odor mapping and classification[27].

Biological sensory pathways further enrich these odor representations through temporal encoding. As illustrated in Figure 1E, neuronal signaling represents sensory inputs as trains of action potentials, in which information is conveyed not only by signal amplitude but also by spike timing and firing rate. Different odorants can induce distinct firing frequencies or temporal patterns, providing an additional coding dimension that enhances separability and robustness against noise[28]. This temporal representation is particularly important in dynamic environments, where stimulus concentration and background conditions fluctuate over time.

In addition to spatial and temporal encoding, synaptic modulation introduces adaptivity and memory into sensory processing. As shown in Figure 1F, repetitive stimulation dynamically modulates excitatory postsynaptic currents (EPSCs), and these changes in EPSC amplitude and dynamics underlie short-term and long-term synaptic plasticity[29]. Through such plasticity, the sensory pathway incorporates stimulus history into its response, enabling habituation, sensitization, and learning. This history-dependent modulation allows biological systems to emphasize salient stimuli while suppressing persistent or irrelevant background signals.

In this context, gas sensors in artificial olfaction naturally implement the receptor function and correspond to the most extensively explored stage of the sensory hierarchy. Neuromorphic artificial olfaction builds upon this foundation by seeking to reproduce not only receptor-level transduction but also the combinatorial, temporal, and plastic coding strategies inherent to biological sensory systems. By incorporating neuron- and synapse-inspired functions, neuromorphic platforms aim to enable encoding, adaptation, and learning to be realized at the hardware level, rather than being confined to purely peripheral or software-based processing[30].

Several sensing approaches have been investigated as potential front ends for artificial olfaction, including electrochemical, optical, acoustic, and catalytic combustion sensors[31,32]. Each type exhibits distinct advantages and limitations depending on operating principles and application conditions. While these modalities can provide high sensitivity or chemical specificity, their deployment in large-scale and densely integrated systems is often constrained by device complexity, peripheral instrumentation, or limited compatibility with standard microelectronic fabrication processes[33].

In contrast, semiconducting metal oxide (SMO)-based chemoresistive gas sensors have been widely adopted owing to a favorable balance between sensing functionality and system-level practicality. Chemoresistive sensors directly transduce chemical interactions at the sensing surface into changes in electrical resistance or conductance, which can be readily interfaced with conventional electronic readout and processing circuitry. This direct electrical transduction enables straightforward integration with on-chip electronics and supports scalable array-level implementations[34,35].

Importantly, the continued relevance of SMO chemoresistive sensors is also rooted in advances in manufacturability and integration strategies, particularly for nanostructured sensing layers[34]. Historically, many SMO sensors were developed as discrete devices with a primary emphasis on sensing performance, often involving high operating temperatures and high-temperature growth or post-deposition treatments that conflicted with CMOS back-end-of-line (BEOL) constraints. Subsequent studies have shown that these limitations are not intrinsic to SMO sensing itself, but rather reflect fabrication paradigms that were not originally designed for monolithic integration.

In response, CMOS-aware manufacturing approaches have been developed to reconcile nanostructured SMO sensing with integrated electronics. At the process level, nanostructured or morphology-engineered SMO sensing layers can be realized using deposition techniques such as sputtering, chemical vapor

deposition, and spray-based methods that are compatible with BEOL thermal budgets and can be implemented at the back end of the CMOS process flow[36,37]. In these approaches, nanostructuring arises from controlled film growth and assembly mechanisms rather than from high-temperature crystal growth. Solution-assisted routes, including spray-based deposition[38,39] and sol-gel processing[40,41], inherently yield porous or nanogranular oxide networks through droplet-mediated deposition, particle nucleation, and interparticle connectivity[42]. Similarly, physical and chemical vapor deposition methods can produce nanocrystalline or columnar morphologies by tuning parameters such as deposition pressure, precursor chemistry, and surface diffusion length, enabling morphology-engineered sensing layers without requiring high-temperature growth or post-CMOS annealing[43].

At the architectural level, fabrication temperature constraints are decoupled from operational requirements by confining elevated temperatures to localized sensing regions during operation, most commonly through integrated microheater and suspended membrane structures[44]. This strategy preserves thermally activated sensing while preventing excessive thermal exposure of surrounding CMOS circuitry, thereby maintaining BEOL integrity and long-term device reliability[34].

Taken together, these attributes position SMO chemoresistive gas sensors as a realistic and scalable front-end technology for artificial olfaction systems. Rather than representing isolated sensing elements, they provide a manufacturable interface between chemical transduction and integrated electronic processing, forming a practical foundation for system-level implementations that extend beyond receptor-level signal acquisition[35,37].

Operation principles and limitations of SMO chemoresistive gas sensors

Conventional SMO chemoresistive gas sensors detect gases through adsorption and redox reactions that modulate carrier concentration and electrical resistance[16,45]. In N-type oxides such as SnO_2, ZnO, and WO_3, oxygen molecules adsorb on the surface and extract electrons from the conduction band, becoming ionized oxygen species[46,47]. This surface process induces an electron depletion layer, creating a core-shell structure with reduced near-surface conductivity. When reducing gases (e.g., CO, H_2, ethanol) are introduced, they react with the ionized oxygen and release trapped electrons back to the semiconductor, narrowing the depletion layer and lowering the resistance [Figure 2A][48,49]. Conversely, oxidizing gases further withdraw electrons and broaden the depletion region, thereby increasing resistance. In P-type oxides such as NiO, CuO, and Co_3O_4, holes act as the majority carriers. Oxygen adsorption leads to the formation of a hole accumulation layer, which contracts when reducing gases supply electrons that neutralize holes, increasing sensor resistance [Figure 2B][50,51]. These mechanisms, grounded in carrier-dependent surface reactions, represent the classical operation of SMO chemoresistive sensors and provide the baseline for further design improvements. Beyond conventional binary oxides, recent efforts have explored multinary and hybrid oxide systems to diversify sensing behavior. Spinel-type oxides (AB_2O_4) allow adjustment of cation distribution between tetrahedral and octahedral sites, offering a means to tune sensing characteristics[52]. Perovskite-type oxides (ABO_3) provide greater structural flexibility through A- and B-site substitution and exhibit distinct response patterns across different analytes[53]. Oxide-oxide heterostructures introduce interfacial charge-transfer effects that influence sensing behavior[54,55], while composite systems combine sensing characteristics from multiple material components[56]. Collectively, these emerging systems extend the material library for neuromorphic olfactory architectures and enable more diverse signal patterns essential for high-dimensional odor representation.

Despite their maturity, such mechanisms face several intrinsic limitations that hinder their applicability in high-performance artificial olfaction. Response and recovery are generally slow at room temperature because the adsorption, ionization, and reaction of oxygen species on oxide surfaces are thermally activated

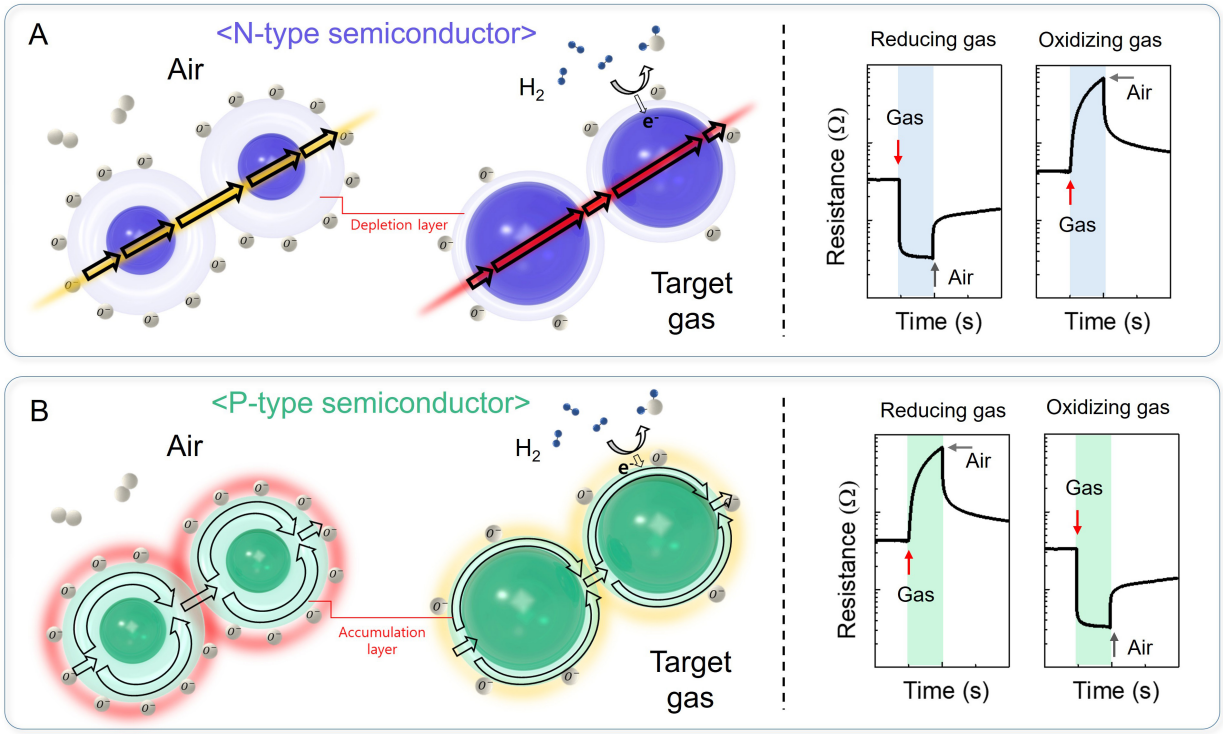

Figure 2. (A and B) Gas sensing mechanism and response curves of n-type and p-type chemoresistive gas sensors.

processes. The insufficient reversibility of these surface reactions leads to progressive signal offsets, which manifest as baseline drift during prolonged operation. These kinetic limitations are strongly temperature-dependent, often necessitating elevated operating conditions to accelerate kinetics and ensure the sufficient formation of reactive oxygen ions[57,58]. However, high-temperature operation substantially increases power consumption and imposes thermal stress on the oxide lattice, while creating compatibility issues with thermally sensitive circuitry in integrated sensor arrays[31,59]. Moreover, when multiple sensors with different operating temperatures are closely integrated, thermal cross-talk and local fluctuations can distort the signals, further complicating calibration and reducing reproducibility. Humidity interference further limits reliability. SMO chemoresistive sensors are highly susceptible to water vapor, which competes with oxygen adsorption and generates surface hydroxyl species that alter surface chemistry[60]. Such interference often obscures the accurate analyte response, particularly under fluctuating environmental conditions, ultimately degrading sensing accuracy. Cross-selectivity also remains a critical challenge. In complex environments containing multiple volatile species, overlapping response signatures severely constrain the discrimination of individual components, especially at trace concentrations (ppm-ppb) relevant for toxic or hazardous gases. This cross-sensitivity reduces recognition accuracy and undermines robustness under realistic conditions[61].

These limitations have motivated a range of material- and device-level strategies aimed at improving the stability and responsiveness of oxide-based sensors[51,54]. The subsequent sections discuss nanostructured architectures that enhance gas accessibility and accelerate reaction kinetics, together with humidity-robust design approaches that stabilize surface chemistry under realistic ambient conditions[62,63]. Alternative emerging mechanisms such as vacancy-mediated chemo-memristive sensing further enable rapid room-temperature operation independent of oxygen-ion kinetics[64]. At the system scale, array-level pattern-recognition and neuromorphic encoding frameworks have also been explored to mitigate cross-selectivity in complex chemical environments.

Performance enhancement via nanostructuring

Optimization of gas-sensing performance is critically influenced by the systematic design of nanostructures. Here, nanostructures serve as the primary platform, as nanoscale dimensional control increases gas-accessible surface area and modifies charge-transport pathways[14,65]. At the fundamental level, nanostructured metal oxides exhibit improved sensing behavior because surface chemical reactions exert a stronger influence on charge transport when characteristic dimensions approach the Debye length[66]. Gas adsorption modulates the electron-depletion or hole-accumulation layer through charge transfer with chemisorbed oxygen species, and reduced dimensions allow this surface-induced band bending to affect a substantial portion of the conduction pathway. In addition, nanostructured frameworks lower diffusion barriers and accelerate adsorption-desorption kinetics, while their dense distribution of undercoordinated atoms and defect sites facilitates rapid surface redox reactions. Collectively, these effects amplify conductivity modulation, resulting in higher sensitivity and faster response and recovery compared to bulk oxides.

While these effects are common to nanostructured oxides, their manifestation depends on structural dimensionality. Figures 3A-C present representative one-dimensional (1-D), two-dimensional (2-D), and three-dimensional (3-D) oxide nanostructures, respectively. 1-D nanostructures, such as nanorods, nanowires, and nanofibers [Figure 3A], impose a geometric constraint in which both gas transport and electrical conduction are largely confined along a single dominant axis[67]. This configuration contrasts sharply with conventional nanoparticle films, where gas diffusion and charge transport occur through tortuous, multidirectional pathways formed by densely packed aggregates[68]. In 1-D architectures, the elongated morphology suppresses severe aggregation and reduces the number of interparticle junctions, leading to a sensing layer with relatively open void space and continuous conduction paths. From a mass-transport perspective, this geometry lowers diffusion resistance by providing low-tortuosity pathways, allowing changes in gas concentration to be more promptly reflected in the electrical response[69]. From an electrical perspective, charge transport proceeds along a limited number of relatively uniform percolative channels, minimizing spatial averaging over heterogeneous grain-boundary barriers[70]. Because surface reactions and charge transport are both constrained along well-defined paths, gas-induced perturbations propagate efficiently through the sensing element. These characteristics are commonly reflected in short response and recovery times and stable response profiles under repeated operation. Rather than producing the largest possible steady-state resistance change, 1-D architectures preferentially emphasize kinetic aspects of the sensing process, such as how rapidly the signal evolves following gas exposure or removal. These characteristics make 1-D nanostructures particularly suitable for sensing scenarios where rapid detection and consistent dynamic behavior are more critical than maximizing signal amplitude.

2-D nanostructures, including nanosheets and nanoflakes [Figure 3B], exhibit a fundamentally different sensing regime arising from their planar geometry and extremely large exposed surface area relative to thickness[71,72]. In these architectures, the conduction pathway is compressed into a thin layer that lies near the gas-solid interface over an extended lateral area. Consequently, a substantial fraction of charge carriers is directly influenced by surface chemical reactions. In aggregated nanoparticle films, gas-solid interactions are often limited to the outer surface of secondary particles, leaving the interior regions electrically inactive. In contrast, thin 2-D architectures enable more efficient utilization of surface-active regions across the entire sensing layer[68]. Variations in surface coverage or reaction rate therefore lead to pronounced modulation of carrier density throughout the conduction pathway, resulting in substantial changes in electrical resistance. In this surface-dominated regime, the sensing response is governed primarily by the extent of surface adsorption and the equilibrium established between gas-phase species and surface sites. As a result, 2-D nanostructures typically exhibit large steady-state resistance modulation and high sensitivity to analyte concentration, with signal magnitude serving as a dominant performance metric[73]. However, because the response is less limited by deep diffusion into the sensing layer, transient kinetic features are generally less

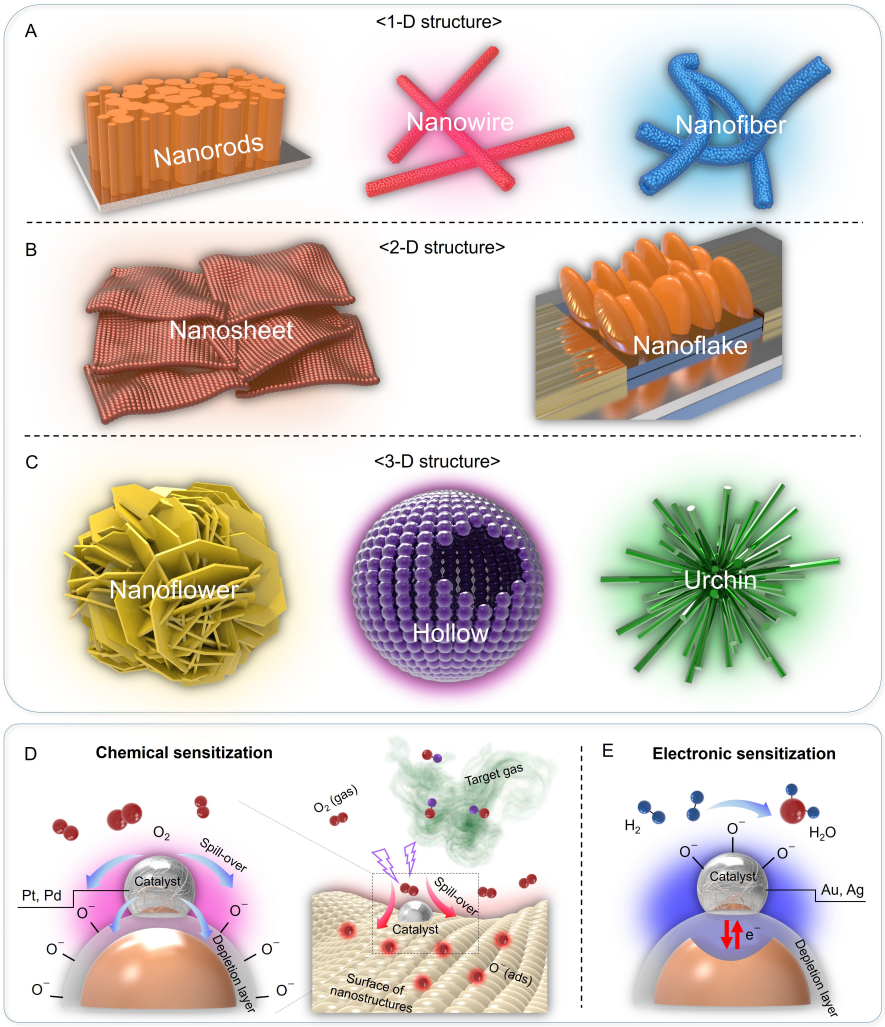

Figure 3. (A-C) Schematic representations of representative 1-D, 2-D, and 3-D oxide nanostructures, including (A) nanorods, nanowires, and nanofibers (B) nanosheets and nanoflakes, and (C) nanoflower-like, hollow, and urchin-like architectures. Schematic illustrations of (D) chemical sensitization and (E) electronic sensitization, highlighting the roles of catalytic reactions and charge transfer in enhancing gas-sensing performance. 1-D: one-dimensional; 2-D: two-dimensional; 3-D: three-dimensional.

pronounced than in 1-D architectures. Accordingly, 2-D nanostructures are particularly advantageous for applications that require accurate concentration-dependent readout and strong signal amplitude, rather than rapid temporal discrimination[67].

3-D nanostructures, such as nanoflower-like, hollow, and urchin-like architectures [Figure 3C], introduce an additional level of structural complexity by organizing low-dimensional nano-building blocks into porous, spatially extended frameworks. Unlike 1-D or 2-D architectures, 3-D structures expose both external and internal surfaces and incorporate interconnected pore networks that allow gas molecules to penetrate deeply into the sensing layer[74]. This structural arrangement substantially increases the effective interaction volume, enabling a larger number of reactive sites to participate in gas-solid interactions. At low analyte concentrations, where the probability of gas-surface encounters is inherently limited, such an increase in accessible surface area and penetration depth becomes particularly important for generating a detectable electrical response[75]. Moreover, the coexistence of pores, edges, junctions, and regions with different local curvature creates spatially heterogeneous adsorption environments within the same sensing element. Consequently, gas exposure induces a collective electrical response arising from multiple local reaction sites

with different characteristic reaction rates and charge-transfer efficiencies[76]. Instead of a uniform response governed by a single dominant mechanism, 3-D architectures integrate contributions from distributed regions throughout the structure. This often leads to broader and more complex response characteristics, especially when compared to the more uniform responses of 1-D and 2-D structures. Such behavior is advantageous in sensing contexts where response diversity and robustness under dilute or complex gas environments are prioritized over optimizing a single performance parameter.

Taken together, these comparisons indicate that nanostructural dimensionality primarily governs how gas-induced perturbations are transduced into electrical signals. 1-D architectures favor rapid sensing responses enabled by directional transport, 2-D architectures amplify surface-controlled signal magnitude through planar conduction, and 3-D architectures increase the effective interaction volume through porous frameworks that support spatially distributed responses. This structure-dependent specialization provides a clear basis for selecting nanostructures according to specific sensing objectives, rather than pursuing a single architecture as a universal solution.

Although nanostructuring is widely employed to enhance sensitivity and signal-to-noise ratio (SNR) in semiconducting metal oxide (SMO) gas sensors by increasing surface-to-volume ratio and amplifying surface-controlled charge modulation, it can also introduce additional sources of device-to-device variation, particularly when implemented over large areas[77]. Such variability originates from the intrinsic complexity of nanostructure formation processes. Spatial fluctuations in nucleation density, growth kinetics, precursor transport[78], and local surface energetics can lead to morphological inhomogeneities across nominally identical devices, manifesting as variations in porosity, grain size distribution, junction density, and local connectivity within the sensing layer[79].

These morphological variations directly translate into electrical non-uniformity in chemoresistive devices. Because gas sensing in SMO materials is governed by surface adsorption, depletion-layer modulation, and potential barriers[80] formed at grain boundaries and interparticle junctions, variations in structural connectivity and surface accessibility result in fluctuations in baseline resistance, response amplitude, and dynamic characteristics[81] such as response and recovery behavior. In large-scale arrays, such statistical dispersion can degrade reproducibility, complicate calibration, and ultimately limit reliable pattern recognition and learning in neuromorphic olfactory systems.

To mitigate these effects at the fabrication level, improved morphological uniformity can be achieved by regulating nucleation and growth kinetics through controlled precursor chemistry, deposition temperature, and growth time, as well as by employing template-assisted or self-assembly-based alignment strategies[82]. In addition, deposition techniques with precise thickness and stoichiometric control, such as atomic layer deposition (ALD) and sputtering, have been shown to reduce dispersion in grain size, porosity, and junction density, thereby suppressing device-to-device variation across large substrates. These fabrication-oriented approaches provide a practical pathway for improving array-level uniformity without fundamentally compromising the sensitivity advantages afforded by nanostructured SMO sensing layers.

While nanostructuring provides an effective means to improve gas accessibility and charge transport, further enhancement of sensing performance requires active control over surface reaction pathways and signal transduction efficiency. Such control can be achieved through nanostructure-catalyst integration, in which noble or transition metals are selectively introduced onto oxide nanostructures. Metal decoration generates localized catalytic sites that accelerate gas adsorption and dissociation processes, while simultaneously modulating interfacial charge transfer and reaction kinetics at the metal-oxide junction[83,84]. Importantly, the role of catalysts in chemoresistive gas sensors extends beyond merely accelerating reaction kinetics.

Depending on the nature of the metal catalyst and its interaction with the oxide support, catalyst-induced enhancement can be understood through two distinct, though complementary, sensitization mechanisms[85]: chemical sensitization and electronic sensitization, schematically illustrated in Figure 3D and E.

Chemical sensitization arises when the catalyst actively participates in the activation of gas-phase species by providing energetically favorable adsorption sites that lower the activation barrier for molecular adsorption, dissociation, or partial activation. As schematically illustrated in Figure 3D, this process is most commonly exemplified by oxygen activation in chemoresistive oxide sensors. Noble metals such as Pd or Pt strongly adsorb O_2 molecules and promote their dissociation into chemisorbed oxygen species, for example O^-, which subsequently migrate from the catalyst surface onto the oxide sensing layer through spillover processes[86,87]. More generally, spillover is not limited to oxygen-derived species but refers to the migration of activated intermediates formed on the catalyst surface to the oxide support. Through this mechanism, the chemically active region extends from the catalyst into the surrounding oxide surface, increasing the population of reactive surface species that participate in gas-solid reactions. By decoupling the initial activation step from the intrinsic surface reactivity of the oxide, chemical sensitization shifts the rate-limiting process toward surface reaction kinetics rather than adsorption probability. Consequently, this mechanism predominantly governs reaction dynamics and selectivity, and its influence is frequently reflected in accelerated response and recovery behavior as well as preferential sensitivity toward gas species that interact strongly with the catalyst surface[14].

Electronic sensitization [Figure 3E], in contrast, originates from electronic interactions at the metal-oxide interface rather than from direct catalytic participation in gas dissociation. Noble metals such as Au or Ag can induce pronounced charge redistribution when interfaced with semiconducting oxides[88,89], leading to local band bending and the formation or modulation of interfacial potential barriers. These electronic perturbations modify the depletion or accumulation profile near the surface, thereby amplifying the conductance change induced by surface reactions. In this mechanism, the catalyst functions primarily as an electronic modulator that enhances the efficiency with which surface chemical events are transduced into an electrical signal[85], even when the intrinsic surface chemistry of the oxide remains largely unchanged.

These mechanistic considerations explain the widespread use of catalyst decoration in enhancing the sensing performance of nanostructured SMO sensors. Chemical sensitization primarily improves how efficiently surface reactions are initiated and sustained by facilitating adsorption, activation, and the availability of reactive intermediates at the sensing interface[90], whereas electronic sensitization strengthens the conversion of those surface events into measurable conductance changes by modulating local band bending and interfacial barriers[91]. Together, these catalyst-induced pathways broaden the controllable parameter space of chemoresistive sensing beyond what can be achieved by nanostructuring alone, enabling more deliberate tuning of key sensing characteristics such as sensitivity, selectivity, and operational stability under realistic conditions[92]. In this context, Table 1 summarizes representative performance metrics reported for nanostructured SMO sensors, encompassing both catalyst-free and catalyst-integrated designs.

A Several representative systems highlight this design principle. Figure 4A shows vertically aligned SnO_2 nanorods fabricated by glancing angle deposition (GLAD), which were functionalized with bimetallic nanocatalysts consisting of Au/Pt and Cu/Ni[133]. The porous nanorod array provided efficient gas diffusion pathways, while the catalyst layer regulated interfacial reactions, resulting in distinct response patterns and markedly enhanced sensitivity toward volatile organic compounds[134]. Such tunability across channels enabled robust discrimination within sensor arrays.

Table 1. Overview of gas sensors based on 1D, 2D, and 3D oxide nanostructures

Dimension	Sensing material	Catalyst material	Target gas	Detection limit	Response/Recovery time	Operating temperature	Ref
1-D							
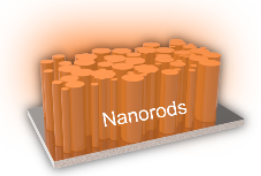	TiO_2	-	n-butanol	144 ppb	73 s/32 s (500 ppm n-butanol)	RT	[93]
	In_2O_3	-	Ethyl acetate	525 ppb	1.8 s/1,748.2 s (100 ppm ethyl acetate)	350 °C	[94]
	In_2O_3	Sn	NO_2	100 ppb	22 s/21 s (50 ppm)	RT	[95]
	WO_3	-	NO_2	-	90 s/150 s (5 ppm NO_2)	RT	[96]
	ZnO	Ag - Ru	CH_4	1 ppm-	18 s/27 s (CH_4 100 ppm)	200 °C	[97]
	SnO_2	-	CO	1 ppm	17 s/- (30 ppm CO)	300 °C	[98]
	CuO	-	O_3	50 ppb	-	100 °C	[99]
	V_2O_5	-	NH_3	-	139 s/2,083 s (500 ppm NH_3)	RT	[100]
	WO_3	CeO_2 nanoparticles	Ethanol	5 ppm	-	250 °C	[101]
	ZnO	NiO foam	Ethylene glycol	500 ppb	4 s/26 s (100 ppm ethylene glycol)	175 °C	[102]
	ZnO	-	NO	500 ppb	358 s/191 s (500 ppb)	200 °C	[103]
	WO_3	Au	N_2O	2.5 ppm	-	250 °C	[104]
	$ZnFe_2O_4$	-	n-Butanol	100 ppb	11 s/-	150 °C	[105]
	WO_3	Pd	Methanol	55 ppb	187 s/-	350 °C	[106]
	Co_3O_4 /In_2O_3	-	Acetone	10 ppb	3 s/6 s (1 ppm acetone)	200 °C	[107]
2-D							
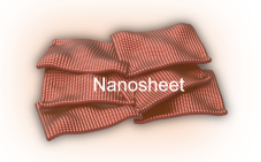	CeO_2	-	HCHO	8.86 ± 0.45 ppm	71 s/310 s (100 ppm HCHO)	250 °C	[108]
	In_2O_3	-	H_2S	0.092 ppb	300 s/300 s (50 ppb H_2S)	37 °C	[109]
	ZnO	-	NO_2	2 ppb	-	250 °C	[110]
	In_2O_3/ZnO	-	H_2S	10 ppm	24 s/27 s	250 °C	[111]
	N doped-ZnO	-	2-Butanone	10 ppm	66 s/236 s (100 ppm butanone)	130 °C	[112]

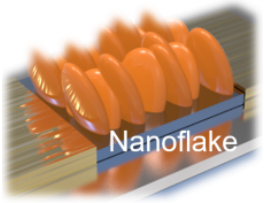	WO_3	Pd	H_2	-	44.2 s/2.7 s	400 °C	[113]
	NiO/Gr-8	-	H_2S	10 ppb	100 s (50 ppm H_2S)/ 7s (100 ppm H_2S)	92 °C	[114]
	Mn doped-ZnO	-	Ethanol	5 ppm	18 s/40 s (50 ppm ethanol)	RT	[115]
	In_2O_3	Pt	Isoprene	2 ppb	-	200 °C	[116]
	V_2O_5	-	NO_2	413 ppt	410 s/1,986 s (20 ppm NO_2)	170 °C	[117]
3-D							
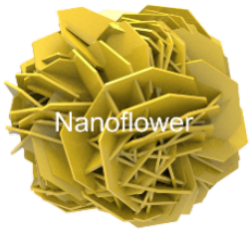	SnO_2	Cu	Ethanethiol	1 ppm	90 s/120 s (10 ppm ethanethiol)	RT	[118]
	ZnO	Pd nanoparticles	TEA	500 ppb	9 s/1,114s (50 ppm TEA)	250 °C	[119]
	SnO_2	Fe	n-Propanol	5 ppb	13.5 s/134.6 s (50 ppm n-propanol)	250 °C	[120]
	Zn mixed-WO_3	-	NO_2	1 ppm	4.21 s/150.66 s (100 ppm NO_2)	150 °C	[121]
	SnO_2	Ag	NO_2	10 ppb	1.4 s/- (100 ppm NO_2)	RT	[122]
	$PrFeO_3$	-	n-Butanol	26.3 ppb	18 s/13 s (100 ppm n-butanol)	280 °C	[123]
	In_2O_3	Au nanoparticles	n-Butanol	50 ppb	8 s/15 s (100 ppm n-butanol)	325 °C	[124]
	ZnO	Au nanoparticles	n-Butanol	100 ppb	1 s/92 s (100 ppm n-butanol)	275 °C	[125]
	V_2O_5	-	Ethanol	100 ppb	63 s/347 s (100 ppm ethanol)	240 °C	[126]
	Bi_2O_3 modified-In_2O_3	Pt nanoparticles	TEA	100 ppb	1 s/- (100 ppm TEA)	140 °C	[127]
	$W_{18}O_{49}$	-	TEA	1 ppm	9 s/147 s (100 ppm TEA)	260 °C	[128]
	CuO	-	NO_x	50 ppb	1 s /78 s	RT	[129]
	ZnO	-	HCHO	298 ppb	448 s/836 s	225 °C	[130]
	WO_{3-x}	-	Linalool	150 ppb	19 s/5 s	275 °C	[131]
	ZnO/SnO_2	-	NO_2	50 ppb	-	100 °C	[132]

1-D: one-dimensional; 2-D: two-dimensional; 3-D: three-dimensional; RT: room temperature; TEA: triethylamine.

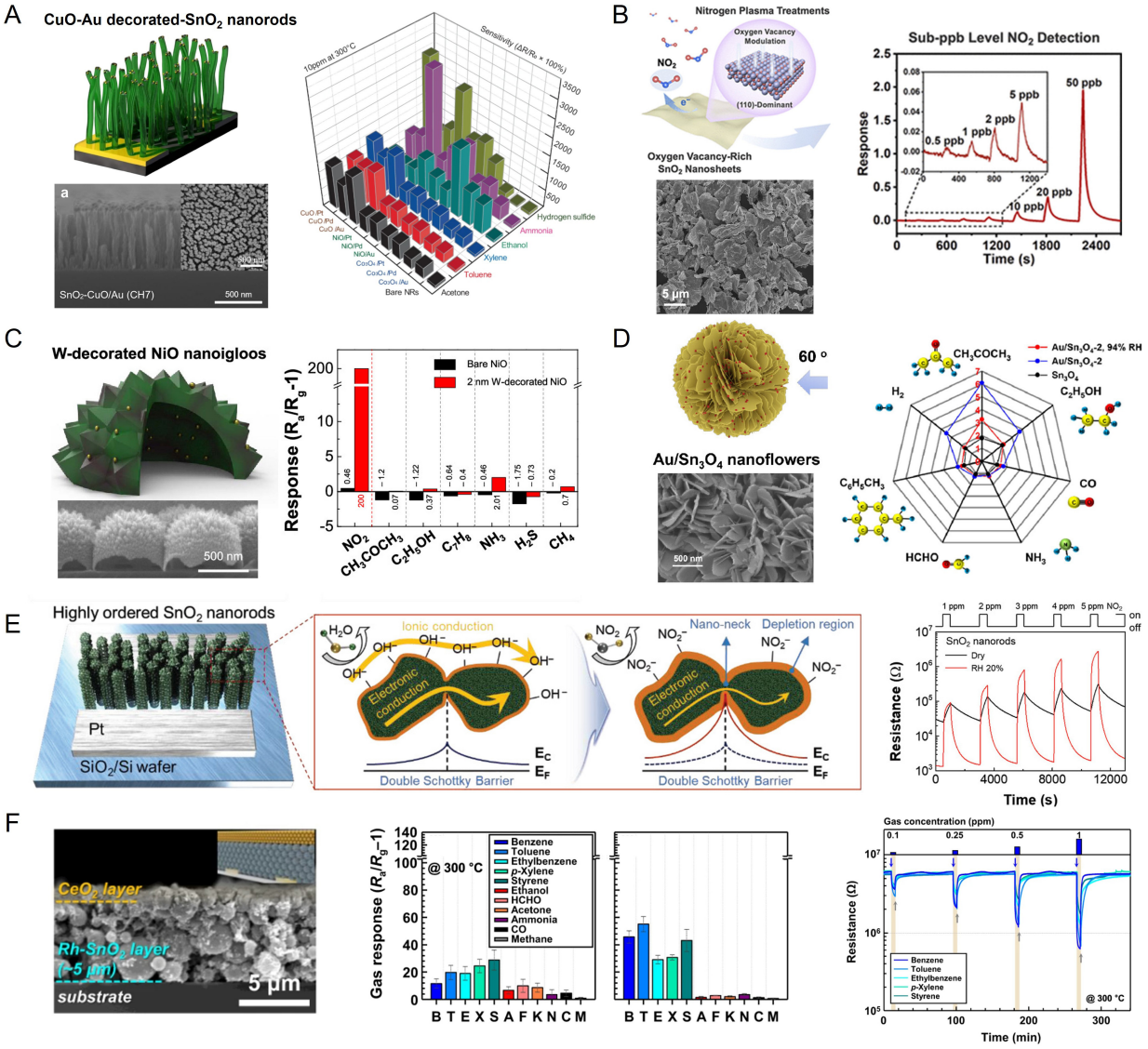

Figure 4. (A) Schematic illustration of SnO_2 nanorods functionalized with Au-CuO composite nanocatalyst via GLAD, along with the corresponding cross-sectional and top-view scanning electron microscopy (SEM) images. Sensitivity of 1 nm-deposited sensor array to six gases (10 ppm acetone, toluene, xylene, ethanol, ammonia, H_2S) at 300 °C. Reprinted with permission. Copyright 2024[133], Springer Nature; (B) Schematic and SEM images of oxygen vacancy-rich SnO_2 nanosheets. Dynamic response-recovery curves of SnO_2 nanosheets after nitrogen plasma treatment for 2.5 min upon exposure to 0.5-50 ppb NO_2 at 80 °C. Reprinted with permission. Copyright 2025[135], American Chemical Society (ACS); (C) Schematic and a cross-sectional SEM image of W-decorated NiO nanoigloos with a bar graph showing the response of bare and W-decorated NiO nanoigloos to various target gases at 300 °C. Reprinted with permission. Copyright 2019[137], American Chemical Society (ACS); (D) Schematic and SEM image of Au-decorated Sn_3O_4 nanoflowers with response values of Sn_3O_4 sensors at 190 °C and Au/Sn_3O_4 sensors at 160 °C to 5 ppm acetone and interfering biomarker gases. Reprinted with permission. Copyright 2024[139], American Chemical Society (ACS); (E) Schematic of NO_2 sensing on the oxygen-adsorbed and hydroxide-functionalized SnO_2 surface. Response curves to 1-5 ppm NO_2 in dry and RH 20% conditions. Reprinted with permission. Copyright 2019[7], Wiley; (F) Cross-sectional SEM image and gas-sensing performance of the 0.4CeO_2/Rh-SnO_2 sensor, along with dynamic response transients to 0.1-1 ppm benzene, toluene, ethylbenzene, xylenes, styrene (BTEXS) at 300 °C. Reprinted with permission. Copyright 2023[149], Springer Nature. GLAD: Glancing angle deposition.

An alternative design strategy is illustrated in Figure 4B, where oxygen vacancy-rich SnO_2 nanosheets were engineered via nitrogen plasma treatment[135]. The nitrogen plasma exposure enabled effective modulation of surface defect chemistry while preserving the two-dimensional nanosheet morphology. The increased density of oxygen vacancies provided abundant active sites for NO_2 adsorption and facilitated charge transfer at the gas-solid interface, resulting in pronounced and reproducible sensing responses. Consequently, the

optimized SnO_2 nanosheets exhibited clear dynamic response-recovery behavior toward 0.5-50 ppb NO_2 at a low operating temperature of 80 °C[136].

In another approach, hollow NiO nanoigloos were synthesized using a soft-template method and subsequently modified with W [Figure 4C][137]. The porous nanoigloo framework already offered a high surface area, but W incorporation generated a rough pyramidal surface enriched with oxygen vacancies. This structural transformation facilitated the formation of NiO/WO_3 heterojunctions, which activated charge transport pathways and enhanced surface reactivity toward NO_2. As a result, the modified structures displayed responses several hundred times higher than pristine NiO[138], while also exhibiting superior selectivity and accelerated response and recovery dynamics.

Au-decorated Sn_3O_4 nanoflowers provide a further example prepared hydrothermally [Figure 4D][139]. The hollow, flower-like assembly of nanosheets created a three-dimensional porous network that facilitated rapid gas diffusion. Au decoration promoted oxygen dissociation and activation, yielding a high density of chemisorbed oxygen species. These effects accelerated redox reactions with acetone, generating extensive conductivity modulation and enabling ppb-level detection limits. Devices based on this architecture achieved rapid response and recovery, while maintaining strong selectivity even under humid conditions.

Beyond structural and catalytic approaches, humidity, traditionally regarded as a detrimental factor due to water poisoning, remains a significant reliability concern in oxide-based chemiresistors. Moisture adsorption generates hydroxyl species and perturbs ionized oxygen equilibria, which can induce baseline drift and reduce gas response. Reported mitigation strategies include incorporating dopants or secondary oxides such as NiO[140], Sb[141], Pd[142] and CuO[143] to suppress humidity-dependent surface reactions[140-146], as well as applying selective porous coatings, including zeolitic imidazolate framework (ZIF) layers[147], to limit moisture uptake while maintaining analyte accessibility. System-level correction using auxiliary humidity readouts and algorithmic post-processing offers an additional layer of compensation. While these approaches improve stability, each introduces trade-offs such as altered selectivity, diffusion limitations, or increased calibration demand, indicating that humidity robustness remains an active design consideration for artificial olfaction. In parallel, recent studies have shown that humidity can under certain conditions participate in ion-activated sensing pathways and even enhance gas response[148]. This humidity-assisted behavior is exemplified in Figure 4E, which highlights an ion-activated sensing mechanism operating under moderate relative humidity. In ion-activated mechanisms, illustrated in Figure 4E, water molecules adsorb and dissociate on oxide nanostructure surfaces, such as SnO_2 nanorods, forming a hydroxide layer that serves as an ionic conduction path[7]. When NO_2 is introduced, this hydroxide layer reacts with the gas molecules, eliminating the ionic mediator and thereby increasing the resistance. Figure 4E schematically depicts this process, while the corresponding measurements demonstrate a pronounced resistance change with rapid recovery under moderate relative humidity, in contrast to the slow and incomplete response observed under dry conditions. This approach converts ambient humidity from an interfering variable into a functional component, enabling room-temperature operation, accelerated response and recovery, and improved selectivity.

Selective filtering strategies offer another dimension of performance enhancement. A representative case is illustrated in Figure 4F, where a nanometer-thick cerium oxide (CeO_2) catalytic overlayer is deposited on an oxide semiconductor sensing film, forming a bilayer structure[149]. Aromatic hydrocarbons, such as benzene, toluene, ethylbenzene, xylene, and styrene, are highly toxic indoor pollutants that occur at trace ppm levels and pose significant health risks. However, they are challenging to detect due to their low reactivity and the presence of interfering gases in indoor air. The CeO_2 overlayer functions as a molecular filter: highly reactive interferents are oxidized into CO_2 and H_2O at the outer layer, while less reactive aromatic hydrocarbons

permeate into the inner oxide sensing film. This bilayer design offers ~ 44-fold higher selectivity toward aromatic hydrocarbons, enabling both qualitative and quantitative discrimination within sensor arrays. Because the CeO_2 overlayer can be applied to various oxide channels, this strategy represents a versatile route to enhance the accuracy and reliability of artificial olfaction under complex environments.

Collectively, these material- and structure-level strategies demonstrate how nanostructured oxide sensors can be engineered to improve selectivity, robustness, and discrimination capability[150] at the sensing stage. Even in such advanced implementations, these approaches primarily address performance optimization at the level of chemical sensing. Within the context of neuromorphic olfaction, conventional nanostructure-based SMO sensors are primarily positioned as sensory front-end components, corresponding to the receptor stage in biological systems[23]. Their contribution is largely confined to the transduction of chemical stimuli into electrical signals, and research efforts have therefore concentrated on optimizing material composition, nanostructure, and interfacial properties to enhance sensitivity, selectivity, and response characteristics at this sensing level. Neuromorphic artificial olfaction, however, is not achieved by signal transduction alone. In biological sensory pathways, receptor-level signals are subsequently structured, encoded, and dynamically modulated through neuronal and synaptic processes[151,152]. Translating these principles into artificial systems requires functional elements that extend beyond the sensing front end, enabling distributed encoding, temporal signal processing, and adaptive modulation[153,154]. In this context, nanostructure-based sensors constitute an essential starting point, while additional functional layers are required to realize neuromorphic-level olfactory processing[155].

INTEGRATION INTO NEUROMORPHIC OLFACTORY ARCHITECTURES

Neuromorphic artificial olfaction aims to emulate the biological pathway, where odorant molecules are converted into electrical signals, organized into combinatorial maps, and processed through networks that exhibit spatiotemporal spiking dynamics and synaptic plasticity. Reproducing these functions in engineered platforms requires oxide nanostructures to serve as versatile building blocks that can underpin odor mapping, spike generation, and adaptive learning within scalable device frameworks.

Recent progress illustrates several complementary directions. Odor map construction has been pursued through the use of sensor arrays that capture chemical diversity and project it into multidimensional patterns for the recognition and discrimination of mixtures[156]. Spike-based signal encoding has been advanced by integrating oxide sensors with neuron circuits, where gas-induced resistance variations regulate leaky integrate-and-fire dynamics, producing analyte-specific temporal codes suitable for processing by spiking neural networks[28]. In parallel, an ion-redox-driven chemo-memristive paradigm exploits defect modulation in oxide channels to generate programmable conductance shifts analogous to synaptic weight updates, thereby embedding sensing with plasticity at the device level[18].

Odor map construction with combinatorial oxide nanostructures

Odor map construction represents a distinct avenue toward neuromorphic olfaction, in which chemical information is captured as spatially distributed patterns rather than temporal dynamics. Oxide nanostructures provide a versatile platform for this strategy, as their compositional diversity can be engineered to yield a wide range of chemical reactivities.

One notable implementation integrated chemoresistive oxide sensors with optoelectronic readout units to realize a compact LED-CMOS-based sensing platform[157]. Figure 5A illustrates the chemical light-emitting diode (ChemLED) architecture, where nanostructured sensing channels are paired with light-emitting diodes, and gas adsorption alters their resistance, thereby modulating the emission intensity of individual pixels. The resulting optical signals are collected in parallel through a CMOS array, enabling scalable, rapid,

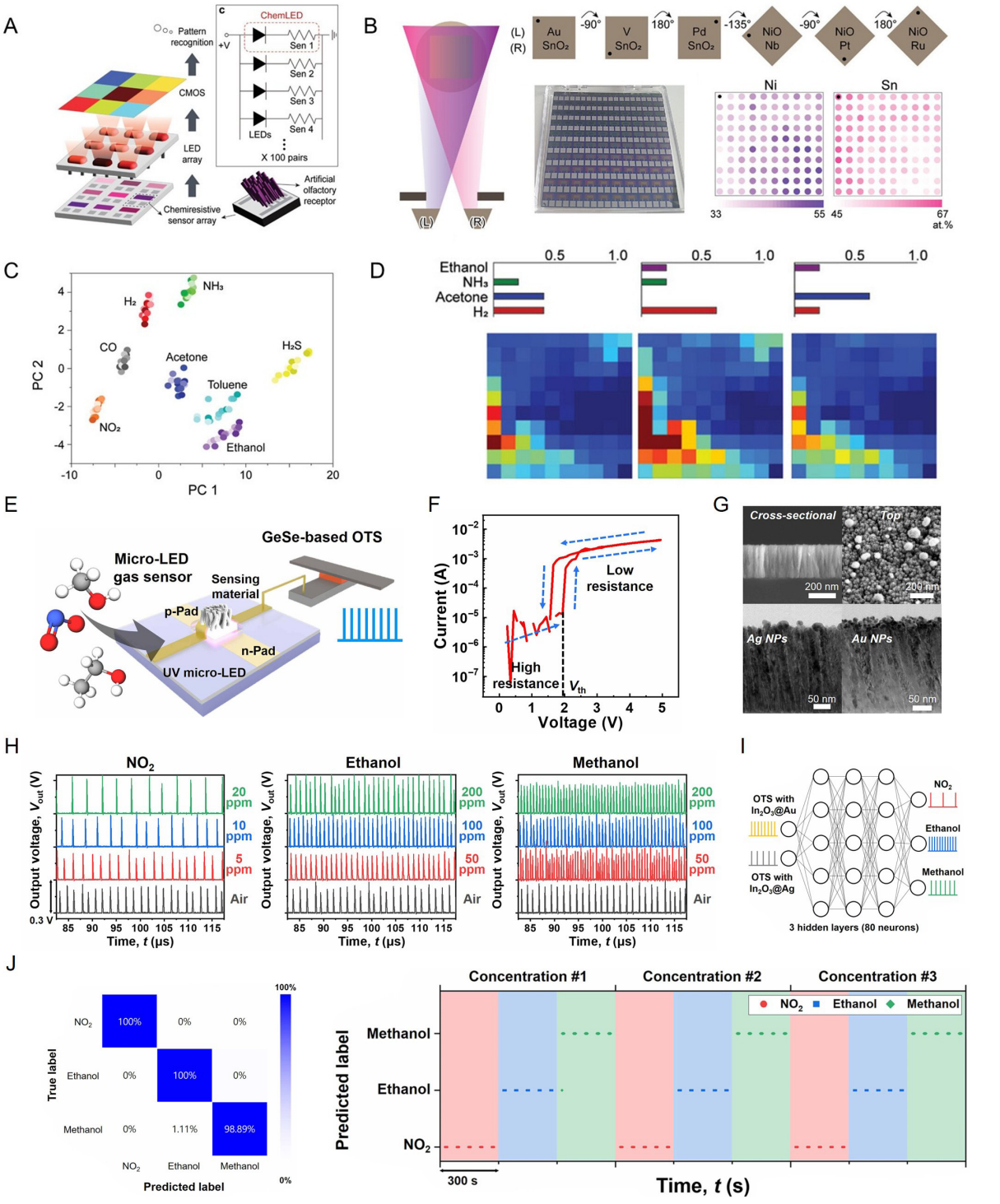

Figure 5. (A) Optical nose system: a chemoresistive nanostructure sensor array drives an LED array (ChemLED units) to generate optical patterns captured by CMOS for odor recognition; (B) Combinatorial fabrication of gradient sensing arrays using tilted deposition and shadow masks; energy dispersive X-ray spectroscopy (EDX) confirms spatial elemental gradients; (C) Principal component analysis (PCA) plot showing distinct clustering for eight gases across concentrations; (D) Response maps of representative gas mixtures derived from ChemLED optical intensities. Reprinted with permission. Copyright 2024 (A-D)[157], Wiley; (E) Schematic of the artificial olfactory neuron module integrating a micro-LED gas sensor and GeSe-based OTS neuron; (F) Current-voltage characteristics of the GeSe-based OTS neuron; (G) SEM and TEM images of porous In_2O_3 nanostructures decorated with Ag and Au nanoparticles; (H) Spiking behavior of the In_2O_3@Au-based neuron module under exposure to NO_2, ethanol, and methanol; (I) SNN architecture for real-time gas classification with three hidden layers; (J) Confusion matrix and real-time gas classification results showing 99.6% accuracy. Reprinted with permission. Copyright 2025 (E-J)[28], American Association for the Advancement of Science (AAAS). ChemLED: Chemical light-emitting diode; OTS: ovonic threshold switch; CMOS: complementary metal-oxide-semiconductor; TEM: transmission electron microscopy; SNN: spiking neural network.

and contact-free data acquisition[158].

To maximize sensing diversity, a combinatorial vapor deposition technique based on GLAD was employed to fabricate an array of chemoresistive oxide nanostructures with continuously varying compositions on a single substrate. In this context, the GLAD-based gradient array illustrates how controlled morphological and compositional variation can be deliberately engineered to expand sensing dimensionality and pattern diversity, functioning as an enabling feature rather than a source of device-level inconsistency when appropriately calibrated. As shown in Figure 5B, this gradient array provides hundreds of distinct sensing elements, each exhibiting unique analyte interactions, enabling the platform to operate as a high-dimensional sensor library. This materials-driven approach eliminates the need for discrete fabrication, while optical readout bypasses the wiring complexity that typically limits scalability.

Figure 5C demonstrates the projection of distributed optical responses into principal component space, where well-separated clusters appear for gases such as NH_3, CO, NO_2, ethanol, acetone, and H_2S. Beyond single-analyte recognition, the same framework also resolves mixtures: Figure 5D shows concentration-dependent odor maps reconstructed from spatially encoded patterns, enabling deconvolution of multiple analyte contributions.

These advances demonstrate that oxide nanostructures, when engineered with compositional gradients and combined with optical readout, can generate artificial odor maps in a compact and scalable manner. By capturing chemical diversity in high-dimensional form, such platforms serve as versatile enablers of neuromorphic olfaction capable of mixture recognition and complex pattern discrimination.

Spike-based signal encoding in neuromorphic olfaction

Biological olfactory neurons convert continuous odor stimuli into temporally resolved spike trains by integrating synaptic inputs until the membrane potential reaches a spike initiation threshold. This temporal spiking representation forms the basis of odor encoding in the olfactory pathway. Inspired by such spike-based encoding principles, an artificial olfactory neuron module has been demonstrated that directly couples gas-induced resistance changes to threshold-switching-driven spiking, thereby enabling simultaneous gas sensing and spike generation within a single device[23].

Recent developments have demonstrated fully integrated neuromorphic olfaction systems capable of overcoming the energy and latency constraints of conventional sensor-processor architectures. A representative system architecture is shown in Figure 5E, where a GeSe-based ovonic threshold switch (OTS) is coupled with a μLED-activated In_2O_3 gas sensor to form an artificial olfactory neuron module operating at microwatt power levels[28]. The OTS exhibits threshold switching near 2.0 V, considerably lower than the 5 to 7 V typically required for MOSFET-based neurons, thus enabling low-voltage spiking and reduced power consumption, as illustrated in Figure 5F.

The μLED activates the SMO sensing layer through 395 nm photoexcitation rather than thermal heating, resulting in a power consumption of only 28 to 213 μW. Sensitivity is further enhanced by plasmonic Au or Ag nanoparticles introduced onto the In_2O_3 surface, which promote gas-surface reactions through localized surface plasmon resonance, as shown in Figure 5G.

Exposure to NO_2, ethanol, or methanol modulates the sensor resistance, altering the charging rate of the parasitic capacitance and thereby tuning the OTS neuron's spiking frequency. Oxidizing gases increase resistance and suppress firing, whereas reducing gases decrease resistance and elevate firing frequency. As displayed in Figure 5H, these effects produce distinct transient spiking signatures across gas species and concentrations, enabling rapid identification without the need for full signal stabilization. Functionally, this hybrid element serves as an input neuron for spiking neural networks (SNNs), closely mimicking temporal

coding processes in biological olfaction.

Two such modules, incorporating In_2O_3 @Au and In_2O_3@Ag sensors respectively, provide input spike trains to an SNN comprising three hidden layers with 80 neurons each [Figure 5I]. Training employed spike frequency data sampled during the transient response regime with logarithmic curve-based augmentation. As shown in Figure 5J, the network achieves 99.6 % accuracy across 540 validation cases and correctly resolves both gas type and concentration. The energy cost per spike is 1.94 nJ, placing this approach among the lowest-power artificial olfactory neuron systems reported to date. Collectively, these results demonstrate a neuromorphic olfactory neuron architecture in which gas-surface interactions are directly translated into temporally encoded spike trains, thereby integrating chemical sensing and neural signal generation within a unified hardware module and enabling energy-efficient artificial olfactory processing.

Complementary paradigm: ion-redox-driven chemo-memristive gas sensing for neuromorphic olfaction

Sensor-synapse integration enables simultaneous gas sensing and synaptic operation within a single device, significantly reducing latency and energy consumption[159]. In conventional e-nose systems, signals from a sensor array must be transmitted to an external processor for pattern recognition and learning, which introduces transfer bottlenecks and limits scalability. In sensor-synapse integrated architectures, electrical changes induced by gas exposure are directly converted into real-time synaptic weight modulation. This intrinsic coupling enables in-sensor learning, where sensing, adaptation, and recognition are closely linked, providing a decisive advantage for fast and energy-efficient neuromorphic olfactory systems.

Beyond carrier-dependent mechanisms, valence change mechanism (VCM)-based memristive devices provide a framework for gas sensing. In VCM memristors, electroforming induces oxygen vacancies that form nanoscale conductive filaments, while SET and RESET operations reversibly form and rupture these filaments under bias electroforming step induces oxygen vacancies, forming nanoscale conductive filaments[160]. The chemo-memristive gas-sensing mechanism is fundamentally governed by oxygen vacancy dynamics within filamentary conduction regions, including filament cores and ruptured or constricted gap regions. Upon exposure to H_2, gas-solid redox reactions extract lattice oxygen, generating additional positively charged oxygen vacancies and releasing electrons. Under a positive bias applied to the top electrode, these vacancies electromigrate toward the bottom electrode along the electric field direction, accumulating in the gap region where localized vacancy agglomerates reconstruct percolative conduction pathways[18]. This direct participation of oxygen vacancies in gas reactions naturally imparts memory-like and history-dependent transfer functions, extending gas sensing toward adaptive neuromorphic behaviors.

A representative implementation is the Pt/TiO_2 nanorod/TiN crossbar structure [Figure 6A][18]. The vertically aligned nanorods define ultrashort conduction channels of ~10 nm, providing a high surface-to-volume ratio and confining switching pathways that are well suited for vacancy-mediated dynamics. Prior to electroforming, the device operates through conventional charge-transfer processes at the oxide surface [Figure 6B]. After electroforming, however, its behavior transitions to ion-redox-driven chemo-memristive dynamics, in which gas exposure induces vacancy generation at ruptured filament sites, yielding type-independent responses [Figure 6C].

Under repeated hydrogen exposure, the device exhibits hysteretic behavior [Figure 6D] demonstrating history-dependent synaptic plasticity. As illustrated in Figure 6E, gas-driven redox reactions directly induce paired-pulse facilitation (PPF) under reducing conditions and paired-pulse depression (PPD) under oxidizing conditions, establishing key synaptic functions. These PPF/PPD dynamics emerge with high linearity and reproducibility [Figure 6F]. Spatially resolved gas-response data [Figure 6G] provide a basis for

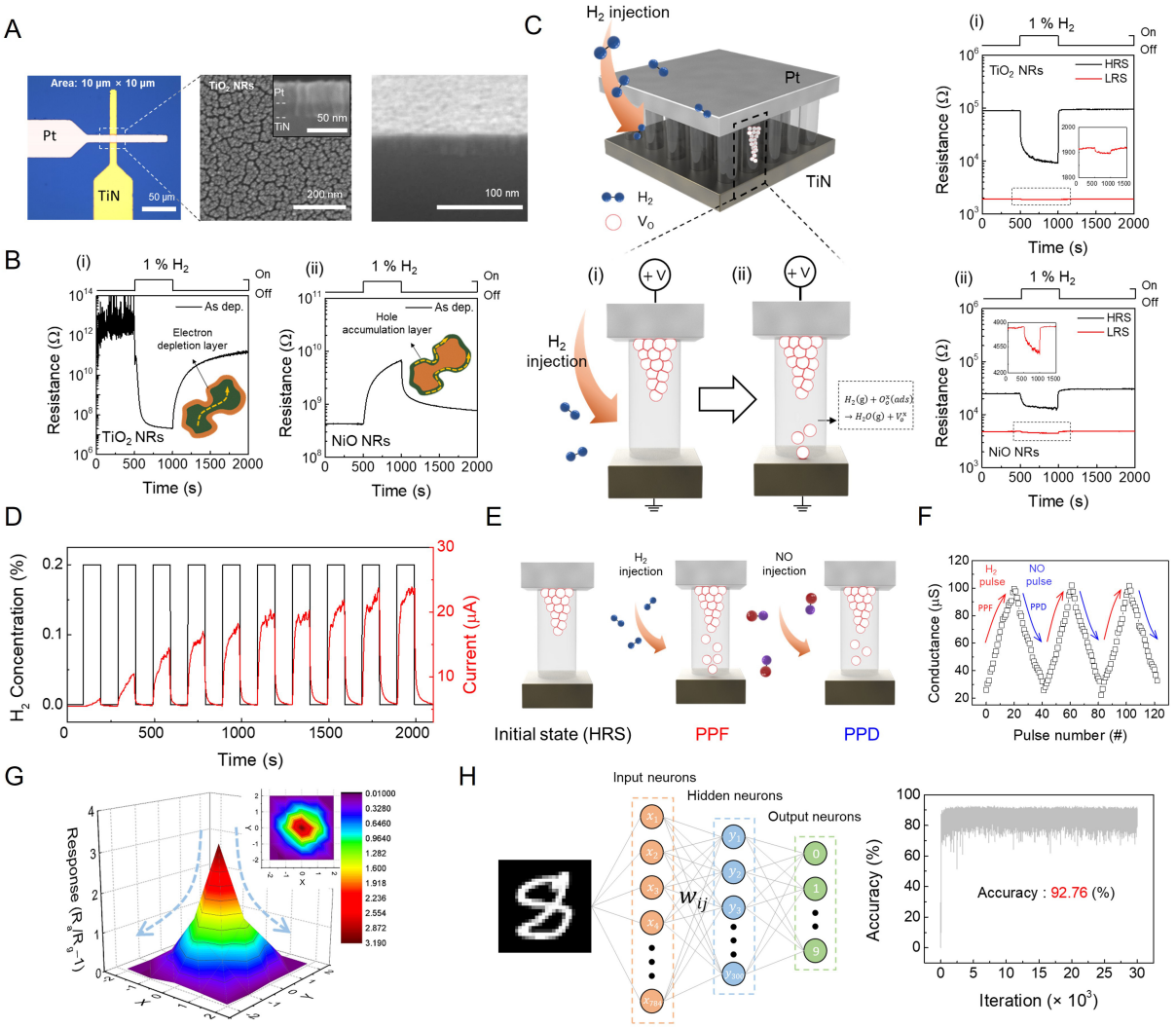

Figure 6. (A) Schematic and SEM images of the chemo-memristive gas sensor, showing the Pt/TiO_2 nanorod/TiN crossbar structure and the highly porous morphology of TiO_2 nanorods; (B) Response curves of TiO_2 nanorods and NiO nanorods upon exposure to 1% H_2 before electroforming; (C) Schematic illustration of the sensor response to H_2 in the initial state and after the formation of oxygen vacancies induced by the reaction with H_2. Response curves of TiO_2 nanorods and NiO nanorods in high resistance state (HRS) and low resistance state (LRS) (red line in inset); (D) Hysteretic response curve of TiO_2 nanorods to 10 consecutive 0.2% H_2 pulses after electroforming; (E) Schematic illustration of controlling the synaptic weights based on the generation and elimination of oxygen vacancies using different target gases; (F) Three sequential conductance modulations based on the type of target gas (reducing or oxidizing); (G) 3D image of the trend in sensor response measured at 25 different locations; (H) MNIST-based neural network simulation for gas generation location inference and corresponding recognition accuracy (~ 92.76%). Reprinted with permission. Copyright 2023(A-H)[18], Wiley. Distributed under the terms of the CC BY-NC-ND license. No modifications have been made to the original images. PPF: Paired-pulse facilitation; PPD: paired-pulse depression; SEM: scanning electron microscopy; MNIST: Modified National Institute of Standards and Technology.

system-level analysis that reflects realistic olfactory input patterns. The Modified National Institute of Standards and Technology (MNIST) dataset is employed to assess the ability of the chemo-memristive platform to learn and classify generic spatial patterns that conceptually mirror the distributed response profiles of gas-sensor arrays. Classification tests using this dataset yield high accuracy, highlighting the potential of the system for reliable neuromorphic olfactory processing [Figure 6H]. Overall, vacancy-mediated filament dynamics in VCM-based chemo-memristive devices unify gas sensing behavior and synaptic functionality, providing a device-level framework for neuromorphic olfactory sensing.

This vacancy-mediated device-level framework has also been realized in alternative chemo-memristive architectures, further clarifying the role of oxygen vacancy redistribution and filament evolution in

gas-responsive synaptic behavior. In addition to chemo-memristive responses originating from high-resistance states, where reducing gases promote additional oxygen vacancy formation in partially ruptured filamentary regions, recent studies have discussed a complementary operating regime in which gas interactions occur in a low-resistance state with a continuous filamentary conduction path[161]. In $Ti/TiO_2/Pt$ crossbar architectures, porous oxide morphologies enable gas-accessible pathways and support vacancy-controlled resistive switching behavior[19].

Under repeated NO_2 exposure, hysteretic behavior exhibits history-dependent synaptic plasticity associated with cumulative oxygen vacancy redistribution in response to gas stimuli. Oxygen vacancy annihilation modifies filamentary and percolative conduction characteristics, leading to conductance evolution governed by prior gas exposure history. Together with the nanorod-based systems discussed earlier, these results demonstrate that chemo-memristive gas sensors share a common physical basis based on oxygen vacancy dynamics and ion migration, while allowing diverse structural implementations. Such platform-level flexibility supports the integration of gas sensing, memory, and synaptic functionality within artificial olfactory systems.

Material and device-level challenges

Oxide nanostructures have progressively transformed artificial olfaction, carrying the field from classical chemoresistive sensing toward architectures that approach neuromorphic function. Early SMO platforms established surface charge-modulated resistance, but limitations in response/recovery speed, selectivity, and environmental robustness hindered their practical impact. Through nanostructuring, catalytic decoration, and interfacial engineering, these limitations have been partially alleviated by improving gas accessibility, surface reaction kinetics, and transduction efficiency, thereby establishing oxide nanostructures as a core material platform for artificial olfaction.

However, these achievements have not eliminated core challenges. Conventional chemoresistive sensing is still fundamentally governed by thermally activated surface reactions and charge transfer, which impose intrinsic limits on response dynamics, particularly under low-temperature or fluctuating environmental conditions[162]. Humidity and background gas interference continue to affect baseline stability and signal reproducibility, while the structural complexity of nanostructured sensing layers can introduce device to device variation that complicates large-area array integration. Taken together, these challenges indicate that material and device engineering, while substantially improving sensing performance, remain primarily focused on receptor-level transduction.

System-level integration and outlook

A further progression in the field is the transition from improved transduction toward integrated processing. To establish a coherent system level perspective, Figure 7 summarizes the general characteristics of three representative neuromorphic implementation pathways: odor map architectures[157,163], hybrid sensor neuron systems[23,28,159], and chemo memristive platforms[18,19]. The comparison is organized around five metrics, including system complexity, adaptive learning capability, energy consumption, integration density, and scalability.

Odor map architectures rely on compositional gradient arrays or optical readouts that generate high dimensional chemical representations, offering strong discrimination capability and intuitive spatial encoding of odor space[157]. These approaches typically employ illumination sources and imaging hardware, which contribute to a higher power footprint but also enable stable, parallel acquisition of rich spatial information. The reliance on spatially distributed structures or optical instrumentation is an inherent aspect of this sensing paradigm, and accordingly these platforms are often implemented with larger physical layouts

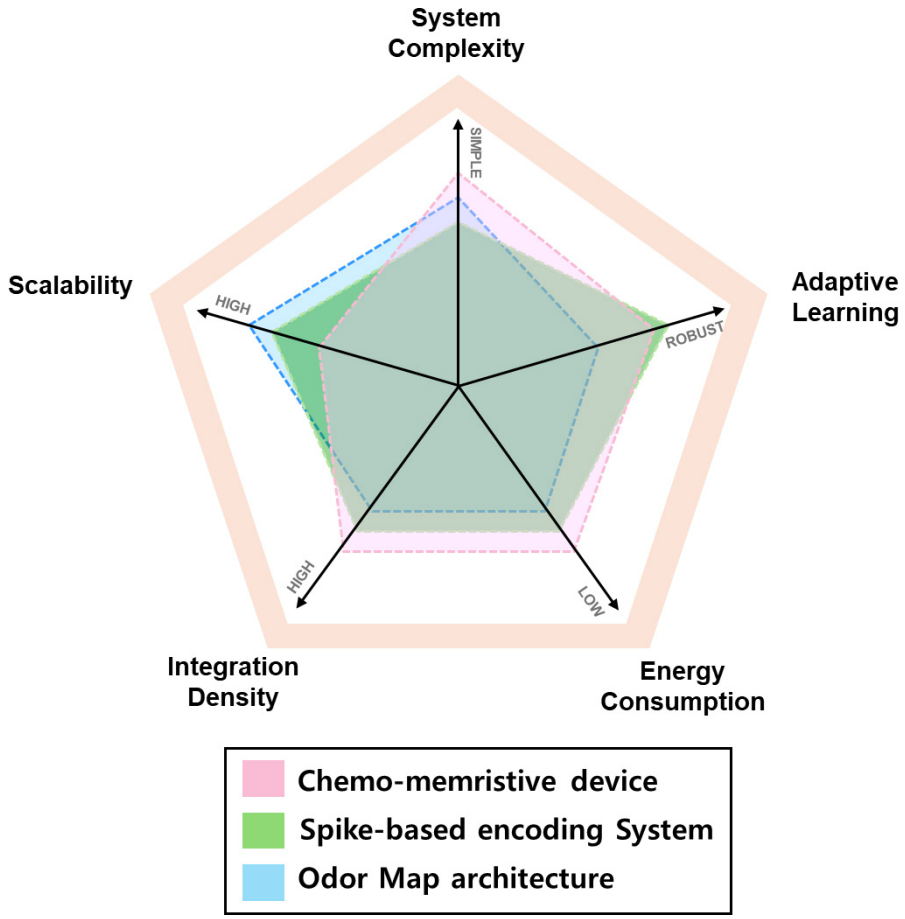

Figure 7. Schematic illustration of summarized general characteristics of three representative neuromorphic olfaction implementation pathways, corresponding to their respective performance in system complexity, adaptive learning capability, energy consumption, integration density, and scalability.

or auxiliary optical components, reflecting architectural characteristics that differ from compact chip level realizations.

Hybrid sensor neuron systems convert gas induced resistance changes into spike trains, enabling temporally precise and event driven encoding[28]. This architecture effectively captures fast transients, allows flexible tuning of neuronal thresholds, and interfaces naturally with neuromorphic readout circuits, providing a versatile route for time resolved odor representations. Their power characteristics are shaped primarily by the microheater operation typically used in SMO sensing layers, although the event driven spiking scheme helps reduce continuous electrical readout demands. In these systems, adaptive behavior is implemented through peripheral neuron circuitry rather than within the sensing medium, a design feature that integrates consistently with larger system architectures.

Chemo-memristive platforms integrate chemical transduction with history dependent conductance modulation within a single device[18]. This built in plasticity enables locally adaptive behavior without additional circuitry, thereby reducing system complexity and supporting high integration density. These devices can operate at room temperature, which removes the need for thermal activation. However, endurance limitations and device to device variability across large arrays still represent practical challenges that influence long term scalability. These distinctions define the broader architectural landscape of neuromorphic olfaction and clarify how different hardware routes partition sensing, encoding, and adaptive

processing across the system.

Moving toward large-scale implementation depends less on advancing each function separately than on developing strategies that co-assemble sensing and processing within a unified oxide-based framework. Such integration offers a realistic route toward dense arrays with simplified calibration and compact, energy-efficient neuromorphic olfactory systems[164].

CONCLUSION

Oxide nanostructures have emerged as a core platform for artificial olfaction, bridging conventional chemoresistive sensing and neuromorphic architectures. Beyond enhancing sensitivity, selectivity, and stability through structural and catalytic engineering, recent developments demonstrate system-level integration strategies, including structured odor representation and spike-based encoding inspired by biological circuits. At the device level, chemo-memristive systems further reveal how sensing, memory, and adaptive dynamics can converge within a single oxide framework. Together, these advances point toward compact, adaptive, and scalable artificial olfactory systems that unify chemical transduction and neuromorphic processing.

DECLARATIONS

Authors' contributions

Conceived and wrote the manuscript: Chun, S. Y.
Reviewed the manuscript: Cho, H. Y.; Shin, H. J.
Supervised the review and finalized the manuscript: Kang, C. Y.; Yoon, J. H.

Availability of data and materials

Not applicable.

AI and AI-assisted tools statement

Not applicable.

Financial support and sponsorship

This research was supported by the National R&D Program through the National Research Foundation of Korea (NRF), funded by the Ministry of Science and ICT (RS-2024-00406418, RS-2024-00403917, and RS-2025-02215065), and the Korea Institute of Science and Technology (26E0181)

Conflicts of interest

All authors declared that there are no conflicts of interest.

Ethical approval and consent to participate

Not applicable.

Consent for publication

Not applicable.

REFERENCES

1. Barnum, G.; Hong, E. J. Olfactory coding. *Curr. Biol.* **2022**, *32*, R1296-301. DOI PubMed PMC
2. Zarzo, M. The sense of smell: molecular basis of odorant recognition. *Biol. Rev.* **2007**, *82*, 455-79. DOI
3. Park, C. O.; Fergus, J. W.; Miura, N.; Park, J.; Choi, A. Solid-state electrochemical gas sensors. *Ionics* **2009**, *15*, 261-84. DOI
4. Paliwal, A.; Sharma, A.; Tomar, M.; Gupta, V. Carbon monoxide (CO) optical gas sensor based on ZnO thin films. *Sensor. Actuat. B-Chem.* **2017**, *250*, 679-85. DOI

5. Li, X.; Sun, W.; Fu, W.; et al. Advances in sensing mechanisms and micro/nanostructured sensing layers for surface acoustic wave-based gas sensors. *J. Mater. Chem. A.* **2023**, *11*, 9216-38. DOI
6. Lee, E.; Hwang, I.; Cha, J.; et al. Micromachined catalytic combustible hydrogen gas sensor. *Sensor. Actuat. B-Chem.* **2011**, *153*, 392-7. DOI
7. Song, Y. G.; Shim, Y. S.; Suh, J. M.; et al. Ionic-activated chemiresistive gas sensors for room-temperature operation. *Small* **2019**, *15*, 1902065. DOI
8. Filipovic, L.; Selberherr, S. Application of two-dimensional materials towards CMOS-integrated gas sensors. *Nanomaterials* **2022**, *12*, 3651. DOI PubMed PMC
9. Jo, Y. K.; Jeong, S.; Moon, Y. K.; Jo, Y.; Yoon, J.; Lee, J. Exclusive and ultrasensitive detection of formaldehyde at room temperature using a flexible and monolithic chemiresistive sensor. *Nat. Commun.* **2021**, *12*, 4955. DOI PubMed PMC
10. Mei, H.; Peng, J.; Wang, T.; et al. Overcoming the limits of cross-sensitivity: pattern recognition methods for chemiresistive gas sensor array. *Nano-Micro. Lett.* **2024**, *16*, 269. DOI PubMed PMC
11. Kaur, N.; Singh, M.; Comini, E. One-dimensional nanostructured oxide chemoresistive sensors. *Langmuir* **2020**, *36*, 6326-44. DOI PubMed PMC
12. Bulemo, P. M.; Cheong, J. Y. Review on porosity control in nanostructured semiconducting metal oxides and its influence on chemiresistive gas sensing. *ACS. Appl. Nano. Mater.* **2023**, *6*, 1027-49. DOI
13. Gao, D. H.; Yu, Q. C.; Kebeded, M. A.; et al. Advances in modification of metal and noble metal nanomaterials for metal oxide gas sensors: a review. *Rare. Metals.* **2025**, *44*, 1443-96. DOI
14. Zhu, L.; Ou, L.; Mao, L.; Wu, X.; Liu, Y.; Lu, H. Advances in noble metal-decorated metal oxide nanomaterials for chemiresistive gas sensors: overview. *Nano-Micro. Lett.* **2023**, *15*, 89. DOI PubMed PMC
15. Das, S.; Mojumder, S.; Saha, D.; Pal, M. Influence of major parameters on the sensing mechanism of semiconductor metal oxide based chemiresistive gas sensors: A review focused on personalized healthcare. *Sensor. Actuat. B-Chem.* **2022**, *352*, 131066. DOI
16. Goel, N.; Kunal, K.; Kushwaha, A.; Kumar, M. Metal oxide semiconductors for gas sensing. *Eng. Rep.* **2022**, *5*, e12604. DOI
17. Yang, X.; Deng, Y.; Yang, H.; et al. Functionalization of mesoporous semiconductor metal oxides for gas sensing: recent advances and emerging challenges. *Adv. Sci.* **2022**, *10*, 2204810. DOI PubMed PMC
18. Chun, S. Y.; Song, Y. G.; Kim, J. E.; et al. An artificial olfactory system based on a chemi-memristive device. *Adv. Mater.* **2023**, *35*, 2302219. DOI
19. Kim, J. S.; Nam, Y.; Kim, D. Y.; et al. Forming-free chemi-memristive gas sensing for artificial olfactory system. *Sensor. Actuat. B-Chem.* **2025**, *444*, 138315. DOI
20. Chen, H.; Li, H.; Ma, T.; Han, S.; Zhao, Q. Biological function simulation in neuromorphic devices: from synapse and neuron to behavior. *Sci. Technol. Adv. Mater.* **2023**, *24*, 2183712. DOI PubMed PMC
21. Chouhdry, H. H.; Lee, D. H.; Bag, A.; Lee, N. A flexible artificial chemosensory neuronal synapse based on chemoreceptive ionogel-gated electrochemical transistor. *Nat. Commun.* **2023**, *14*, 821. DOI PubMed PMC
22. Francia, S.; Lodovichi, C. The role of the odorant receptors in the formation of the sensory map. *BMC. Biol.* **2021**, *19*, 174. DOI PubMed PMC
23. Han, J. K.; Kang, M.; Jeong, J.; et al. Artificial olfactory neuron for an in-sensor neuromorphic nose. *Adv. Sci.* **2022**, *9*, 2106017. DOI
24. Rahimzadeh, H.; Sadeghi, M.; Ghasemi-varnamkhasti, M.; Mireei, S. A.; Tohidi, M. On the feasibility of metal oxide gas sensor based electronic nose software modification to characterize rice ageing during storage. *J. Food. Eng.* **2019**, *245*, 1-10. DOI
25. Cho, W.; Yoon, S.; Chung, T. D. Streamlining the interface between electronics and neural systems for bidirectional electrochemical communication. *Chem. Sci.* **2023**, *14*, 4463-79. DOI PubMed PMC
26. Miura, K.; Mainen, Z. F.; Uchida, N. Odor representations in olfactory cortex: distributed rate coding and decorrelated population activity. *Neuron* **2012**, *74*, 1087-98. DOI PubMed PMC
27. Tang, Y.; Zhou, B.; Liu, J.; et al. Specific odor coding using a single thin-film transistor. *Nano. Lett.* **2025**, *25*, 7587-94. DOI
28. Kang, M.; Han, J. -K.; Lee, K.; et al. Neuromorphic olfaction with ultralow-power gas sensors and ovonic threshold switch. *Sci. Adv.* **2025**, *11*, eadv9222. DOI PubMed PMC
29. Dominguez, K.; Kumbhar, D. D.; Syed, A. M.; Martin, R. C.; El-Atab, N. The evolution of gas sensors into neuromorphic systems. *Adv. Electron. Mater.* **2025**, *12*, e00639. DOI
30. Stasenko, S. V.; Mikhaylov, A. N.; Kazantsev, V. B. Model of neuromorphic odorant-recognition network. *Biomimetics* **2023**, *8*, 277. DOI PubMed PMC
31. Dey, A. Semiconductor metal oxide gas sensors: a review. *Mat. Sci. Eng. B-Adv.* **2018**, *229*, 206-17. DOI
32. Liu, X.; Cheng, S.; Liu, H.; Hu, S.; Zhang, D.; Ning, H. A survey on gas sensing technology. *Sensors* **2012**, *12*, 9635-65. DOI PubMed PMC

33. Gebicki, J.; Szulczynski, B.; Kaminski, M. Determination of authenticity of brand perfume using electronic nose prototypes. *Meas. Sci. Technol.* **2015**, *26*, 125103. DOI
34. Lackner, E.; Krainer, J.; Wimmer-Teubenbacher, R.; et al. Carbon monoxide detection with CMOS integrated thin film SnO_2 gas sensor. *Mater. Today:. Proc.* **2017**, *4*, 7128-31. DOI
35. Suh, J.; Cho, I.; Kang, K.; et al. Fully integrated and portable semiconductor-type multi-gas sensing module for IoT applications. *Sensor. Actuat. B-Chem.* **2018**, *265*, 660-7. DOI
36. Rüffer, D.; Hoehne, F.; Bühler, J. New digital metal-oxide (MO_x) sensor platform. *Sensors* **2018**, *18*, 1052. DOI
37. Park, J.; Park, K.; Kim, T.; Shin, S.; Park, C.; Yoo, H. Three-electrode metal-oxide gas sensor system with CMOS interface IC. *IEEE. Sensors. J.* **2016**, 1. DOI
38. Korotcenkov, G.; Cho, B. Spray pyrolysis deposition of undoped SnO_2 and In_2O_3 films and their structural properties. *Prog. Cryst. Growth. Charact. Mater.* **2017**, *63*, 1-47. DOI
39. Hyodo, T.; Fujii, E.; Ishida, K.; Ueda, T.; Shimizu, Y. Microstructural control of porous In2O3 powders prepared by ultrasonic-spray pyrolysis employing self-synthesized polymethylmethacrylate microspheres as a template and their NO_2-sensing properties. *Sensor. Actuat. B-Chem.* **2017**, *244*, 992-1003. DOI
40. Park, S.; Kim, C.; Lee, W.; Sung, S.; Yoon, M. Sol-gel metal oxide dielectrics for all-solution-processed electronics. *Mat. Sci. Eng. R.* **2017**, *114*, 1-22. DOI
41. Znaidi, L. Sol-gel-deposited ZnO thin films: a review. *Mat. Sci. Eng. B-Adv.* **2010**, *174*, 18-30. DOI
42. Banger, K. K.; Yamashita, Y.; Mori, K.; et al. Low-temperature, high-performance solution-processed metal oxide thin-film transistors formed by a ‘sol-gel on chip’ process. *Nat. Mater.* **2010**, *10*, 45-50. DOI
43. Montero, J.; Ji, Y.; Li, S.; Niklasson, G. A.; Granqvist, C. G. Sputter deposition of thermochromic VO_2 films on In_2O_3:Sn, SnO_2, and glass: structure and composition versus oxygen partial pressure. *J. Vac. Sci. Technol. B:Nanotechnol. Microelectron.* **2015**, *33*, 031805. DOI
44. Lahlalia, A.; Filipovic, L.; Selberherr, S. Modeling and simulation of novel semiconducting metal oxide gas sensors for wearable devices. *IEEE. Sensors. J.* **2018**, *18*, 1960-70. DOI
45. Imash, A.; Smagulova, G.; Kaidar, B.; et al. Chemoresistive gas sensors based on electrospun 1D nanostructures: synergizing morphology and performance optimization. *Sensors* **2024**, *24*, 6797. DOI PubMed PMC
46. Sopiha, K. V.; Malyi, O. I.; Persson, C.; Wu, P. Chemistry of oxygen ionosorption on SnO_2 surfaces. *ACS. Appl. Mater. Interfaces.* **2021**, *13*, 33664-76. DOI
47. Motsoeneng, R. G.; Kortidis, I.; Ray, S. S.; Motaung, D. E. Designing SnO_2 nanostructure-based sensors with tailored selectivity toward propanol and ethanol vapors. *ACS. Omega.* **2019**, *4*, 13696-709. DOI
48. Ahmad, N.; Kanjariya, P.; Priya, G. P.; et al. Recent advances on the gas-sensing properties and mechanism of perovskite oxide materials - a review. *ACS. Omega.* **2025**, *10*, 13780-96. DOI
49. Liu, Y.; Xiao, S.; Du, K. Chemiresistive gas sensors based on hollow heterojunction: a review. *Adv. Mater. Inter.* **2021**, *8*, 2002122. DOI
50. Mori, M.; Noguchi, A.; Itagaki, Y. VOC detections by p-type semiconducting sensors using nano-sized $SmFeO_3$ particles. *Sensors* **2022**, *22*, 5616. DOI
51. Kim, H.; Lee, J. Highly sensitive and selective gas sensors using p-type oxide semiconductors: overview. *Sensor. Actuat. B-Chem.* **2014**, *192*, 607-27. DOI
52. Wu, J.; Gao, D.; Sun, T.; et al. Highly selective gas sensing properties of partially inversed spinel zinc ferrite towards H_2S. *Sensor. Actuat. B-Chem.* **2016**, *235*, 258-62. DOI
53. Chander, S.; Tripathi, S.; Kaur, I. ABO_3-based perovskite oxides for gas sensors: a review of recent advancement in materials, mechanisms, and strategies for real-time applications. *Chem. Eng. J.* **2025**, *524*, 169490. DOI
54. Miller, D. R.; Akbar, S. A.; Morris, P. A. Nanoscale metal oxide-based heterojunctions for gas sensing: a review. *Sensor. Actuat. B-Chem.* **2014**, *204*, 250-72. DOI
55. Shao, F.; Hoffmann, M.; Prades, J.; et al. Heterostructured p-CuO (nanoparticle)/n-SnO_2 (nanowire) devices for selective H_2S detection. *Sensor. Actuat. B-Chem.* **2013**, *181*, 130-5. DOI
56. Kim, J.; Jeong, H.; Na, C. W.; et al. Highly selective and sensitive xylene sensors using Cr_2O_3-$ZnCr_2O_4$ hetero-nanostructures prepared by galvanic replacement. *Sensor. Actuat. B-Chem.* **2016**, *235*, 498-506. DOI
57. Sharma, A.; Eadi, S. B.; Noothalapati, H.; Otyepka, M.; Lee, H.; Jayaramulu, K. Porous materials as effective chemiresistive gas sensors. *Chem. Soc. Rev.* **2024**, *53*, 2530-77. DOI
58. Majhi, S. M.; Mirzaei, A.; Kim, H. W.; Kim, S. S.; Kim, T. W. Recent advances in energy-saving chemiresistive gas sensors: a review. *Nano. Energy.* **2021**, *79*, 105369. DOI

59. Bing, Y.; Zhang, F.; Han, J.; Zhou, T.; Mei, H.; Zhang, T. A method of ultra-low power consumption implementation for MEMS gas sensors. *Chemosensors* **2023**, *11*, 236. DOI
60. Wang, Y.; Zhou, Y. Recent progress on anti-humidity strategies of chemiresistive gas sensors. *Materials* **2022**, *15*, 8728. DOI
61. Turlybekuly, A.; Shynybekov, Y.; Soltabayev, B.; Yergaliuly, G.; Mentbayeva, A. The cross-sensitivity of chemiresistive gas sensors: nature, methods, and peculiarities: a systematic review. *ACS. Sens.* **2024**, *9*, 6358-71. DOI
62. Yu, S.; Jia, X.; Zhang, J.; Yang, W.; Song, H. Recent advances in different materials for moisture resistance of metal oxide-based gas sensors: a review. *Chem. Eng. J.* **2025**, *505*, 159639. DOI
63. Liu, L.; Wang, Y.; Liu, Y.; et al. Heteronanostructural metal oxide-based gas microsensors. *Microsyst. Nanoeng.* **2022**, *8*, 85. DOI
64. Lee, D.; Yun, M. J.; Kim, K. H.; Kim, S.; Kim, H. Advanced recovery and high-sensitive properties of memristor-based gas sensor devices operated at room temperature. *ACS. Sens.* **2021**, *6*, 4217-24. DOI
65. Panžić, I.; Bafti, A.; Radovanović-Perić, F.; et al. Advancements in nanostructured functional constituent materials for gas sensing applications: a comprehensive review. *Appl. Sci.* **2025**, *15*, 2522. DOI
66. Mirzaei, A.; Lee, J.; Majhi, S. M.; et al. Resistive gas sensors based on metal-oxide nanowires. *J. Appl. Phys.* **2019**, *126*, 241102. DOI
67. Kolmakov, A.; Moskovits, M. Chemical sensing and catalysis by one-dimensional metal-oxide nanostructures. *Annu. Rev. Mater. Res.* **2004**, *34*, 151-80. DOI
68. Korotcenkov, G. Gas response control through structural and chemical modification of metal oxide films: state of the art and approaches. *Sensor. Actuat. B-Chem.* **2005**, *107*, 209-32. DOI
69. Fan, Z.; Wang, D.; Chang, P.; Tseng, W.; Lu, J. G. ZnO nanowire field-effect transistor and oxygen sensing property. *Appl. Phys. Lett.* **2004**, *85*, 5923-5. DOI
70. Kirkpatrick, S. Percolation and conduction. *Rev. Mod. Phys.* **1973**, *45*, 574-88. DOI
71. Hübner, M.; Simion, C.; Tomescu-Stănoiu, A.; Pokhrel, S.; Bârsan, N.; Weimar, U. Influence of humidity on CO sensing with p-type CuO thick film gas sensors. *Sensor. Actuat. B-Chem.* **2011**, *153*, 347-53. DOI
72. Moon, C. S.; Kim, H.; Auchterlonie, G.; Drennan, J.; Lee, J. Highly sensitive and fast responding CO sensor using SnO_2 nanosheets. *Sensor. Actuat. B-Chem.* **2008**, *131*, 556-64. DOI
73. Kim, H.; Choi, K.; Lee, J.; Akbar, S. A. Highly sensitive and ultra-fast responding gas sensors using self-assembled hierarchical SnO_2 spheres. *Sensor. Actuat. B-Chem.* **2009**, *136*, 138-43. DOI
74. Qin, L.; Xu, J.; Dong, X.; et al. The template-free synthesis of square-shaped SnO_2 nanowires: the temperature effect and acetone gas sensors. *Nanotechnology* **2008**, *19*, 185705. DOI
75. Zhang, J.; Wang, S.; Wang, Y.; et al. NO_2 sensing performance of SnO_2 hollow-sphere sensor. *Sensor. Actuat. B-Chem.* **2009**, *135*, 610-7. DOI
76. Yoon, J.; Choi, S. H.; Kim, J.; Jang, H. W.; Kang, Y. C.; Lee, J. Trimodally porous SnO_2 nanospheres with three-dimensional interconnectivity and size tunability: a one-pot synthetic route and potential application as an extremely sensitive ethanol detector. *NPG. Asia. Mater.* **2016**, *8*, e244. DOI
77. Zan, H.; Dai, M.; Hsu, T.; Lin, H.; Meng, H.; Yang, Y. Porous organic TFTs for the applications on real-time and sensitive gas sensors. *IEEE. Electron. Device. Lett.* **2011**, *32*, 1143-5. DOI
78. Guo, T.; Yao, M.; Lin, Y.; Nan, C. A comprehensive review on synthesis methods for transition-metal oxide nanostructures. *CrystEngComm* **2015**, *17*, 3551-85. DOI
79. Xiao, X.; Liu, L.; Ma, J.; et al. Ordered mesoporous tin oxide semiconductors with large pores and crystallized walls for high-performance gas sensing. *ACS. Appl. Mater. Interfaces.* **2018**, *10*, 1871-80. DOI
80. Choi, Y.; Hwang, I.; Park, J.; Choi, K. J.; Park, J.; Lee, J. Novel fabrication of an SnO_2 nanowire gas sensor with high sensitivity. *Nanotechnology* **2008**, *19*, 095508. DOI
81. Bhowmik, B.; Fecht, H.; Bhattacharyya, P. Vertical mode gas sensing performance of TiO_2 nanotube array by tuning of surface area and carrier transport length. *IEEE. Sensors. J.* **2015**, *15*, 5919-26. DOI
82. Zhou, J.; Hua, Z.; Liu, Z.; Wu, W.; Zhu, Y.; Shi, J. Direct synthetic strategy of mesoporous ZSM-5 zeolites by using conventional block copolymer templates and the improved catalytic properties. *ACS. Catal.* **2011**, *1*, 287-91. DOI
83. Kim, I.; Rothschild, A.; Tuller, H. L. Advances and new directions in gas-sensing devices. *Acta. Mater.* **2013**, *61*, 974-1000. DOI
84. Baek, J. W.; Kim, I. Advances in perovskite oxides for chemiresistive sensors. *Acc. Mater. Res.* **2023**, *4*, 1108-20. DOI
85. Moseley, P. T. Progress in the development of semiconducting metal oxide gas sensors: a review. *Meas. Sci. Technol.* **2017**, *28*, 082001. DOI
86. Shin, H.; Jung, W.; Kim, D.; et al. Single-atom Pt stabilized on one-dimensional nanostructure support via carbon nitride/SnO_2 heterojunction trapping. *ACS. Nano.* **2020**, *14*, 11394-405. DOI

87. Koo, W.; Cho, H.; Kim, D.; et al. Chemiresistive hydrogen sensors: fundamentals, recent advances, and challenges. *ACS. Nano.* **2020**, *14*, 14284-322. DOI
88. Bezkrovnyi, O.; Bruix, A.; Blaumeiser, D.; et al. Metal-support interaction and charge distribution in ceria-supported Au particles exposed to CO. *Chem. Mater.* **2022**, *34*, 7916-36. DOI
89. Koshevoy, E.; Gribov, E.; Lyulyukin, M.; Selishchev, D.; Kozlov, D. Photoelectrochemical study of M/TiO_2 (M = Pt, Pd, Au) supported catalysts: flat-band potentials and photoelectrocatalytic properties in glycerol oxidation reaction. *J. Photoch. Photobio. A.* **2026**, *471*, 116678. DOI
90. Shin, H.; Ko, J.; Park, C.; et al. Sacrificial template-assisted synthesis of inorganic nanosheets with high-loading single-atom catalysts: a general approach. *Adv. Funct. Mater.* **2021**, *32*, 2110485. DOI
91. Van Tran, T.; Kim, D.; Duc Le, T.; Oh, G.; Shin, G.; Yu, Y. Alloy core composition effect of Pd-Augr-alloy@ZnO core-shell nanoparticles on hydrogen gas sensing performance. *Chem. Eng. J.* **2024**, *483*, 149050. DOI
92. Kim, D.; Kim, J. K.; Oh, D.; et al. Ex-solution hybrids functionalized on oxide nanofibers for highly active and durable catalytic materials. *ACS. Nano.* **2023**, *17*, 5842-51. DOI
93. Li, Y.; Cheng, X.; Zhang, S.; et al. Alcohol selectivity of a room temperature-operated gas sensor based on TiO_2 burr-like nanorods. *Chem. Eng. J.* **2025**, *508*, 160923. DOI
94. Sanghikian Marques Dos Santos, G.; Theodoro, R. D. S.; Gera, G. O.; Micheli Perfecto, T.; Paschoalini Volanti, D. Ethyl acetate detection using mixed-phase In_2O_3 nanorods. *ACS. Appl. Nano. Mater.* **2025**, *8*, 11458-69. DOI
95. Du, Y.; Ren, L.; Yuan, J.; Zhang, R.; Xie, M.; Xu, H. *In-situ* synthesized Sn-doped In_2O_3 nanorods for low-temperature NO_2 sensing with high response. *Sensor. Actuat. B-Chem.* **2025**, *445*, 138564. DOI
96. Kandhare, N.; Mathe, V.; Bhagwat, S. Room temperature NO_2 gas sensor using h-WO_3 nanorod based thin films. *Mat. Sci. Eng. B-Adv.* **2024**, *305*, 117422. DOI
97. Li, X.; Hu, H.; Tan, T.; et al. Enhancing methane gas sensing through defect engineering in Ag-Ru Co-doped ZnO nanorods. *ACS. Appl. Mater. Interfaces.* **2024**, *16*, 26395-405. DOI
98. Jo, M.; Kim, S.; Park, S.; et al. Fast-response and low-power self-heating gas sensor using metal/metal oxide/metal (MMOM) structured nanowires. *ACS Sens.* **2024**, *9*, 1896-905. DOI
99. Lai, L.; Hsueh, H.; Chiu, C.; Cheng, T.; Chang, S. Thermal oxidation CuO nanowire gas sensor for ozone detection applications. *Sens. Actuators. Rep.* **2024**, *8*, 100228. DOI
100. Thi Nguyet, T.; Van Duy, L.; Nam, N. C.; et al. Transition from p-type to n-type semiconductor in V_2O_5 nanowire-based gas sensors: synthesis and understanding of the sensing mechanism. *Sensor. Actuat. B-Chem.* **2025**, *424*, 136841. DOI
101. Malik, S. B.; Mejia-Centeno, K. V.; Martínez-Alanis, P. R.; et al. Synergistic effect of CeO_2 nanoparticles and WO_3 nanowires in gas sensing applications. *Sensor. Actuat. B-Chem.* **2024**, *400*, 134879. DOI
102. Wang, X.; Wang, X.; Sui, X.; et al. ZnO nanowire/NiO foam 3D nanostructures for high-performance ethylene glycol sensing. *Sensor. Actuat. B-Chem.* **2024**, *400*, 134918. DOI
103. Khomarloo, N.; Gidik, H.; Bagherzadeh, R.; et al. Enhancing nitric oxide gas detection by tuning the structural dimension of electrospun ZnO nanofibers fibers and polymers. *Fibers. Polym.* **2024**, *26*, 197-209. DOI
104. To, D. T. H.; Yang, B.; Myung, N. V. Enhancing nitrous oxide chemiresistive sensing performance by reducing ionic Oxygen species adsorption in Gold functionalized Tungsten Trioxide nanofibers. *Sens. Actuators. Rep.* **2024**, *8*, 100255. DOI
105. Luo, Q.; Wan, Y.; Wang, Z.; Gao, S.; Chen, Y.; Feng, C. Excellent-performing gas sensor based on Yttrium-doped $ZnFe_2O_4$ nanofibers for detection of n-Butanol. *J. Alloys. Compd.* **2025**, *1027*, 180605. DOI
106. Kim, Y. W.; Yang, B.; To, D. T. H.; et al. Improved selectivity toward methanol detection via Pd-functionalized tungsten trioxide nanofiber gas sensors. *Chem. Eng. J.* **2025**, *523*, 168814. DOI
107. Wu, J.; Zheng, Z.; Chi, H.; Jiang, J.; Zhu, L.; Ye, Z. Ultrasensitive and exclusive chemiresistors with a ZIF-67-derived oxide cage/nanofiber Co_3O_4/In_2O_3 heterostructure for acetone detection. *ACS. Appl. Mater. Interfaces.* **2024**, *16*, 9126-36. DOI
108. Bhunia, A. K.; Mahata, B.; Mandal, B.; Guha, P. K.; Saha, S. Emerging 2D nanoscale metal oxide sensor: semiconducting CeO_2 nano-sheets for enhanced formaldehyde vapor sensing. *Nanotechnology* **2024**, *35*, 455501. DOI
109. Li, J.; Deng, Y.; Liu, L.; et al. Synthesis of 2D porous indium oxide nanosheets for fabrication of high-performance flexible gas sensors. *Small* **2025**, *21*, e05870. DOI
110. Kim, M. Y.; Choa, H.; Park, C. O.; et al. Boundary engineering of porous zinc oxide nanosheets to enhance gas sensing performance. *Sens. Actuators. Rep.* **2025**, *9*, 100322. DOI
111. Nii Okai Amu-Darko, J.; Hussain, S.; Zhang, X.; et al. Enhanced H_2S gas sensing utilizing UV-assisted In_2O_3@ZnO nanosheets. *Ceram. Int.* **2024**, *50*, 38242-52. DOI

112. Zhang, Y.; Shen, Y.; Zhang, W.; Sun, Z.; Gu, F.; Wang, L. Enhanced low-working temperature 2-butanone gas-sensing performance of N-doped ZnO mesoporous nanosheets. *J. Mater. Sci:. Mater. Electron.* **2024**, *35*, 485. DOI
113. Abedzadeh, M.; Ranjbar, M.; Kameli, P. Fabrication of Pd-decorated tungsten oxide nanoflakes for hydrogen sensors via facile anodizing oxidation method. *Int. J. Hydrogen. Energy.* **2024**, *50*, 1325-34. DOI
114. Yang, M.; Liu, L.; Li, B.; et al. Novel NiO nanoflakes in situ grown on graphene layers for the sensitive detection of low concentration H_2S. *Appl. Surf. Sci.* **2026**, *720*, 165191. DOI
115. Awale, M.; Lokhande, S. D.; Kathwate, L. H.; Vasundhara, M.; Mote, V. D.; Kadam, A. B. Highly sensitive and selective gas sensors for ethanol based on Mn doped ZnO nanoflakes. *J. Cluster. Sci.* **2024**, *35*, 2273-82. DOI
116. Cheng, Y.; Portela, R.; Wang, P.; et al. Ultrasensitive In_2O_3-Based nanoflakes for lung cancer diagnosis and the sensing mechanism investigated by *operando* spectroscopy. *ACS. Sens.* **2024**, *9*, 6382-9. DOI
117. Parveen, R. A.; Vinoth, E.; Archana, J.; Ponnusamy, S.; Navaneethan, M. Highly sensitive parts per trillion detection of microwave assisted V_2O_5 nano-flake sensor for hazardous NO_2. *Chem. Phys.* **2026**, *601*, 112949. DOI
118. Chen, L.; Sun, X.; Song, Z.; Gao, R.; Guo, Z.; Huang, X. Theoretical validation of non-noble Cu sites integrated on SnO_2 nanoflowers for enhanced gas sensing of ethanethiol at room temperature. *Inorg. Chem.* **2024**, *63*, 11438-49. DOI
119. Fu, S.; Wang, A.; Yin, M.; Li, G. Pd nanoparticles decorated 3D peony-like ZnO nanoflowers enable ultra-high response and selectivity of TEA gas sensing: experimental and DFT validation. *J. Alloys. Compd.* **2025**, *1047*, 184972. DOI
120. Li, Y.; Kuang, X.; Yu, L.; et al. Fe sites engineering unlocks selective chemiresistive sensing of n-propanol for breath-based lung cancer diagnostics. *Chem. Eng. J.* **2025**, *521*, 166508. DOI
121. Nimbalkar, T. M.; Kadam, S. A.; Ma, Y.; Selvaraj, M.; Assiri, M. A.; Patil, V. B. Tailoring Zn mixed WO_3 nanoflowers for highly efficient NO_2 gas detection. *Ceram. Int.* **2024**, *50*, 38514-21. DOI
122. Qi, L.; Song, B.; Wu, H.; et al. Synthesis of Ag-doped SnO_2 nanoflowers and applications to room temperature high-performance NO_2 gas sensing. *Sensor. Actuat. B-Chem.* **2024**, *420*, 136494. DOI
123. Ni, P.; Ma, S.; Ma, N.; et al. Porous hollow sphere structure $PrFeO_3$ as an efficient sensing material for n-butanol detection. *J. Alloys. Compd.* **2024**, *1002*, 175392. DOI
124. Wang, G.; Wang, Y.; Guo, L.; et al. Chemiresistive n-butanol gas sensors based on Au@In_2O_3 hollow-sphere-array thin films. *Sensor. Actuat. B-Chem.* **2025**, *422*, 136579. DOI
125. Wang, G.; Chen, T.; Guo, L.; et al. Chemiresistive n-butanol gas sensors based on Co_3O_4@ZnO hollow-sphere-array thin films prepared by template-assisted magnetron sputtering. *Sensor. Actuat. B-Chem.* **2024**, *413*, 135862. DOI
126. Zhang, F.; Qu, Y.; Lu, X.; et al. Double-shelled hollow sphere V_2O_5-based conductometric ethanol gas sensor. *Sensor. Actuat. B-Chem.* **2024**, *417*, 136009. DOI
127. Li, X.; Li, Y.; Xu, X.; et al. Persistently boosted TEA sensing performance of In_2O_3 hollow spheres by sequentially modified with Bi_2O_3 and Pt nanoparticles. *Sensor. Actuat. B-Chem.* **2025**, *422*, 136628. DOI
128. Zhao, Z.; Xu, X.; Zhang, H. Pr-doped $W_{18}O_{49}$ sea urchin-like nanospheres for enhanced triethylamine gas sensor. *Sensor. Actuat. B-Chem.* **2026**, *450*, 139280.
129. Xue, T.; Yu, J.; Yu, H.; et al. Construction of gas-sensing material with ZnO crystal flower clustered on sea urchin-like CuO structure and its gas-sensing properties to NO_x at room temperature. *Ceram. Int.* **2025**, *51*, 42806-14. DOI
130. Zhou, Y.; Luo, Y.; Zheng, Z.; et al. Urchin-like Na-doped zinc oxide nanoneedles for low-concentration and exclusive VOC detections. *J. Adv. Ceram.* **2024**, *13*, 507-17. DOI
131. Cheng, Y.; Teng, Y.; Zheng, M.; et al. 3D Urchin-Like WO_{3-x} based nanostructures with abundant oxygen vacancies for ppb-Level tea aroma sensing. *Sensor. Actuat. B-Chem.* **2024**, *419*, 136293. DOI
132. Sun, Y.; Han, D.; Sun, S.; Dong, Y.; Li, X.; Qian, K. Urchin-like dual-shelled ZnO/SnO_2 hollow spheres for ultrahigh sensitive low-temperature NO_2 sensing. *Sensor. Actuat. B-Chem.* **2026**, *450*, 139227. DOI
133. Sung, S.; Suh, J. M.; Hwang, Y. J.; Jang, H. W.; Park, J. G.; Jun, S. C. Data-centric artificial olfactory system based on the eigengraph. *Nat. Commun.* **2024**, *15*, 1211. DOI
134. Madvar, H. R.; Kordrostami, Z.; Mirzaei, A. Sensitivity enhancement of resistive ethanol gas sensor by optimized sputtered-assisted CuO decoration of ZnO nanorods. *Sensors* **2022**, *23*, 365. DOI
135. Zhai, Y.; Yang, R.; Wu, J.; et al. Nitrogen plasma-driven oxygen vacancy modulation in tin dioxide nanosheets enables sub-parts-per-billion nitrogen dioxide detection at low operating temperature. *ACS. Sens.* **2025**, *10*, 4184-93. DOI
136. Bu, W.; Zhang, Y.; Qin, Q.; et al. Improved ppb-level NO_2 conductometric sensor induced by trace Au on SnO2 nanosheet. *Sensor. Actuat. B-Chem.* **2023**, *379*, 133237. DOI

137. Yi, S. Y.; Song, Y. G.; Park, J. Y.; et al. Morphological evolution induced through a heterojunction of W-decorated NiO nanoigloos: synergistic effect on high-performance gas sensors. *ACS. Appl. Mater. Interfaces.* **2019**, *11*, 7529-38. DOI
138. Li, Q.; Zhang, P.; Ning, T.; et al. Gas sensor based on flower-like NiO modified with WO_3 nanoparticles for NO_2 detection. *ACS. Appl. Nano. Mater.* **2024**, *7*, 7856-64. DOI
139. Hou, J.; Yang, Z.; Rong, Q.; Zhang, C.; Wang, C.; Guo, Y. Au-decorated Sn_3O_4 nanoflower-based MEMS gas sensor for detecting ppb-level acetone. *ACS. Appl. Nano. Mater.* **2024**, *7*, 6506-15. DOI
140. Kim, H. R.; Haensch, A.; Kim, I. D.; Barsan, N.; Weimar, U.; Lee, J. H. The role of NiO doping in reducing the impact of humidity on the performance of SnO_2-based gas sensors: synthesis strategies, and phenomenological and spectroscopic studies. *Adv. Funct. Mater.* **2011**, *21*, 4456-63. DOI
141. Suematsu, K.; Sasaki, M.; Ma, N.; Yuasa, M.; Shimanoe, K. Antimony-doped tin dioxide gas sensors exhibiting high stability in the sensitivity to humidity changes. *ACS. Sens.* **2016**, *1*, 913-20. DOI
142. Ma, N.; Suematsu, K.; Yuasa, M.; Kida, T.; Shimanoe, K. Effect of water vapor on Pd-loaded SnO_2 nanoparticles gas sensor. *ACS. Appl. Mater. Interfaces.* **2015**, *7*, 5863-9. DOI
143. Choi, K.; Kim, H.; Kang, Y. C.; Lee, J. Ultraselective and ultrasensitive detection of H2S in highly humid atmosphere using CuO-loaded SnO_2 hollow spheres for real-time diagnosis of halitosis. *Sensor. Actuat. B-Chem.* **2014**, *194*, 371-6. DOI
144. Kim, J.; Na, C. W.; Kwak, C.; et al. Humidity-independent gas sensors using Pr-doped In_2O_3 macroporous spheres: role of cyclic Pr^{3+}/Pr^{4+} redox reactions in suppression of water-poisoning effect. *ACS. Appl. Mater. Interfaces.* **2019**, *11*, 25322-9. DOI
145. Kwak, C.; Kim, T.; Jeong, S.; Yoon, J.; Kim, J.; Lee, J. Humidity-independent oxide semiconductor chemiresistors using terbium-doped SnO_2 yolk-shell spheres for real-time breath analysis. *ACS. Appl. Mater. Interfaces.* **2018**, *10*, 18886-94. DOI
146. Yoon, J. W.; Kim, J. S.; Kim, T. H.; Hong, Y. J.; Kang, Y. C.; Lee, J. H. A new strategy for humidity independent oxide chemiresistors: dynamic self-refreshing of In_2O_3 sensing surface assisted by layer-by-layer coated CeO_2 nanoclusters. *Small* **2016**, *12*, 4229-40. DOI
147. Yao, M. S.; Tang, W. X.; Wang, G. E.; Nath, B.; Xu, G. MOF Thin film-coated metal oxide nanowire array: significantly improved chemiresistor sensor performance. *Adv. Mater.* **2016**, *28*, 5229-34. DOI
148. Nasriddinov, A.; Rumyantseva, M.; Konstantinova, E.; et al. Effect of humidity on light-activated NO and NO_2 gas sensing by hybrid materials. *Nanomaterials* **2020**, *10*, 915. DOI
149. Jeong, S.; Moon, Y. K.; Wang, J.; Lee, J. Exclusive detection of volatile aromatic hydrocarbons using bilayer oxide chemiresistors with catalytic overlayers. *Nat. Commun.* **2023**, *14*, 233. DOI
150. Sun, Y.; Liu, S.; Meng, F.; et al. Metal oxide nanostructures and their gas sensing properties: a review. *Sensors* **2012**, *12*, 2610-31. DOI
151. Wilson, R. I.; Mainen, Z. F. Early events in olfactory processing. *Annu. Rev. Neurosci.* **2006**, *29*, 163-201. DOI
152. Wachowiak, M.; Shipley, M. T. Coding and synaptic processing of sensory information in the glomerular layer of the olfactory bulb. *Semin. Cell. Dev. Biol.* **2006**, *17*, 411-23. DOI
153. Imam, N.; Cleland, T. A. Rapid online learning and robust recall in a neuromorphic olfactory circuit. *Nat. Mach. Intell.* **2020**, *2*, 181-91. DOI
154. Schmuker, M.; Pfeil, T.; Nawrot, M. P. A neuromorphic network for generic multivariate data classification. *Proc. Natl. Acad. Sci. U.S.A.* **2014**, *111*, 2081-6. DOI
155. Jang, Y. W.; Kim, J.; Shin, J.; et al. Autonomous artificial olfactory sensor systems with homeostasis recovery via a seamless neuromorphic architecture. *Adv. Mater.* **2024**, *36*, 2400614. DOI
156. Raman, B.; Stopfer, M.; Semancik, S. Mimicking biological design and computing principles in artificial olfaction. *ACS. Chem. Neurosci.* **2011**, *2*, 487-99. DOI
157. Kwon, H.; Kamboj, O.; Song, A.; et al. Scalable optical nose realized with a chemiresistively modulated light-emitter array. *Adv. Mater.* **2024**, *36*, 2402287. DOI
158. Xiong, Z.; Liang, W.; Zhang, M.; Mao, D.; Xia, Q.; Xu, G. Parallelizing analog in-sensor visual processing with arrays of gate-tunable silicon photodetectors. *Nat. Commun.* **2025**, *16*, 4728. DOI
159. Lee, S.; Kang, M.; Han, J.; Yun, S.; Park, I.; Choi, Y. An artificial olfactory sensory neuron for selective gas detection with in-sensor computing. *Device* **2023**, *1*, 100063. DOI
160. Chen, J. Y.; Huang, C. W.; Chiu, C. H.; Huang, Y. T.; Wu, W. W. Switching kinetic of VCM-based memristor: evolution and positioning of nanofilament. *Adv. Mater.* **2015**, *27*, 5028-33. DOI
161. Ali, M.; Lee, D.; Ahmad, I.; Kim, H. Recent progress in memristor-based gas sensors (Gasistor; gas sensor + memristor): device modeling, mechanisms, performance, and prospects. *Sens. Actuators. Rep.* **2025**, *9*, 100269. DOI
162. Najafi, P.; Ghaemi, A. Chemiresistor gas sensors: design, challenges, and strategies: a comprehensive review. *Chem. Eng. J.* **2024**, *498*, 154999. DOI

163. Wang, Y.; Li, R.; Xin, S.; et al. An artificial optical nose integrated by metal-organic frameworks three-dimensional photonic crystal array for identification of trace hazardous gases through machine learning integration. *J. Environ. Chem. Eng.* **2025**, *13*, 117043. DOI

164. Dennler, N.; True, A.; Van Schaik, A.; Schmuker, M. Neuromorphic principles for machine olfaction. *Neuromorph. Comput. Eng.* **2025**, *5*, 023001. DOI